UAV-Enabled Image Capture and Wireless Delivery for On-Demand Surveillance Tasks

Nguyen Van Cuong, *Member, IEEE*, Y.-W. Peter Hong, *Senior Member, IEEE*, and Jang-Ping Sheu, *Fellow, IEEE*

***Abstract*— This work examines the task assignment, transmission scheduling, and trajectory design of image-surveillance UAVs dispatched to serve on-demand image capture and delivery services to ground users, e.g., from drivers seeking images of traffic jams or security units requesting images of private homes. In each task, the UAVs are required to capture the image of a specified surveillance region and deliver the image to the requesting user before the deadline. The task assignment, transmission scheduling, and trajectory design are jointly determined to maximize the total surveillance area of the completed tasks. We first examine the single-UAV problem and propose an alternating optimization approach that adopts the exact penalty method to promote near-binary solutions and employ successive convex approximation to deal with the nonconvex trajectory optimization. Then, we extend to the multiple-UAV scenario where cross-UAV tasks may require images to be captured and delivered by different UAVs. To enable distributed implementation, we introduce auxiliary deadlines to limit the time available for local tasks and, thus, decouple the joint optimization problem into multiple single-UAV problems that can be solved in parallel following the procedure derived in the previous case. Numerical simulations are provided to demonstrate the effectiveness of the proposed solutions.**

***Index Terms*— Image surveillance UAVs, wireless delivery, trajectory optimization, transmission scheduling, task assignment.**

I. Introduction

THE use of unmanned aerial vehicles (UAVs) to capture and deliver images serves a key role in many different applications, such as traffic monitoring [1], border patrol [2], structural inspections [3], agriculture surveillance [4], and search and rescue [5]. Due to the swift deployment and movement, image surveillance UAVs can fly quickly to target regions to take timely aerial images of ground events and provide a first-person view of the events to the users requesting the service. The high flexibility and fast response time are difficult to achieve by fixed camera systems or photographers on the ground. For example, in traffic monitoring [1], UAVs can monitor highways, intersections, or road segments with high traffic volume and provide real-time information through aerial images to facilitate traffic management. In border patrol [2], UAVs can provide coverage over wide areas or geographically hazardous regions that are otherwise difficult to access by human security guards. In these applications, task assignment and transmission scheduling are essential for efficiently completing image surveillance tasks but can be challenging due to the widely spread surveillance areas and requesting users.

The trajectory design and resource allocation of image surveillance UAVs have been examined in several recent works, e.g., [5], [6], [7], [8], and [9]. For example, in [5], multiple image surveillance UAVs were considered for rescue operations. The UAVs' trajectories were jointly designed to maximize the nonredundant data of photographs taken over specific sensing locations. Reference [6] determined the coverage path of an image surveillance UAV while considering the speed, acceleration, and energy of the UAV and the resolution constraint of the images. Reference [7] determined the UAV trajectory by minimizing the total travel distance required to complete all image capture tasks, taking into account the minimum resolution of the captured images. Moreover, in [8], UAVs were used for outdoor crowd surveillance in situations such as the COVID-19 pandemic prevention. The images were analyzed to detect and locate individuals in the intended area. In [9], multi-purpose UAVs were dispatched to perform image surveillance and relay communication for ground users simultaneously. The collected data contained both the ground users' uplink data and the images captured by the onboard camera. The objective was to maximize the sum-log-throughput of the ground users under both image surveillance and relay communication constraints. In addition to image surveillance, other modes of sensing by the UAV, e.g., radio sensing, have also been examined in the literature. For example, [10] considered the joint optimization of the UAVs' trajectories, including speed and direction, sensing locations, and transmission scheduling, to minimize the completion time of given tasks. A sense-and-send protocol was proposed that allowed UAVs to perform data sensing and data transmission sequentially. The order in which the tasks are served was assumed to be known a priori, and the sensory data was sent to a common base station. In [11], a UAV was used to provide downlink service to ground users while simultaneously

Manuscript received 13 May 2023; revised 13 November 2023 and 2 February 2024; accepted 4 May 2024. Date of publication 14 May 2024; date of current version 11 October 2024. This work was supported in part by the National Science and Technology Council, Taiwan, under Grant 111-2221-E-007-042-MY3 and Grant 112-2811-E-007-036-MY3. The associate editor coordinating the review of this article and approving it for publication was H. Zhang. *(Corresponding author: Y.-W. Peter Hong.)*

Nguyen Van Cuong and Jang-Ping Sheu are with the Institute of Communications Engineering and the Department of Computer Science, National Tsing Hua University, Hsinchu 30013, Taiwan (e-mail: cuongnv@gapp.nthu.edu.tw; sheujp@cs.nthu.edu.tw).

Y.-W. Peter Hong is with the Institute of Communications Engineering, National Tsing Hua University, Hsinchu 30013, Taiwan (e-mail: ywhong@ee.nthu.edu.tw).

Color versions of one or more figures in this article are available at https://doi.org/10.1109/TWC.2024.3397951.

Digital Object Identifier 10.1109/TWC.2024.3397951

utilizing radio signals to sense ground targets. The user association, sensing time decision, beamforming vector, and UAV's trajectory were jointly determined to maximize the users' downlink rates under constraints on the targets' sensing frequencies and beam pattern gains. While the above works also focused on image surveillance and sensing applications, they did not take into consideration the timeliness of the delivery and the heterogeneity of the delivery location.

The existence of heterogeneous deadlines for different tasks poses additional challenges to the UAV's trajectory design and resource allocation and has also been examined recently in, e.g., [12], [13], [14], [15], and [16]. In these works, the time available for completing different tasks may affect the priorities of their assignments. In [12], UAVs were deployed to perform time-constrained data collection from the Internet-of-Things (IoT) devices. The UAV trajectory and resource allocation were jointly determined by maximizing the number of IoT devices served. By considering a non-orthogonal multiple access (NOMA) transmission scheme, [13] also aimed to maximize the number of IoT devices served by optimizing the UAV's trajectory, scheduling, and power allocation. In this case, the NOMA clustering, IoT devices' deadlines, and the UAV's power consumption were further considered in the design. Moreover, in the context of mobile edge computing, [14] considered the offloading of computing tasks from IoT devices to UAVs under deadline constraints. Reference [15] studied the UAV trajectory optimization in a time-constrained data collection application where data was gathered at a single base station. The objective was to minimize the completion time under the age of information and energy consumption constraints. The UAV's velocity was optimized using a successive convex approximation approach, and the genetic algorithm was adopted to find the optimal visiting order. [16] considered a similar problem where the UAV collected data from IoT devices during their respective time windows and relayed the information to a single base station. The UAV trajectory, bandwidth, and power allocation were jointly determined by maximizing the number of served IoT devices, considering the UAV's capacity limitation and the IoTs' data amount. In the above works, UAVs received data from the IoT devices over wireless links instead of capturing data directly by onboard cameras or sensors. The constraints in the latter case may be more stringent, making the task assignment more challenging to do efficiently. Moreover, the time and communication resources required to deliver the collected data to the end terminals were often neglected. The possibility of having multiple delivery locations for different tasks was also not considered.

Several recent works have also investigated the use of multiple cooperative UAVs for wireless delivery, e.g., [17], [18], [19], and [20]. For example, in [17], UAVs were used to form a multi-hop link between remote IoT devices and a data sink node. The UAVs' energy consumption was minimized by jointly determining their transmission schedules and transmit powers while ensuring the time constraint of the data delivery task. Note that the UAVs' data collection behavior and trajectory designs were not examined in their work. Reference [18] investigated a similar problem where the data collected by UAVs were sent either directly to the base station or passed to other UAVs at pre-defined meeting points. The transmission schedule was determined by maximizing the minimum battery level among all UAVs at the end of the mission. Reference [19] studied the cooperative transport of data from sensing locations to a base station by multiple UAVs. Their goal was to minimize the transmission latency by choosing appropriate meeting times and locations between UAVs. In [20], UAVs were assigned both individual and common sensing tasks. In the latter case, information about the target location was repeatedly sensed and transmitted to the base station by multiple UAVs. By viewing UAVs as a virtual antenna array, the task assignment and transmit power allocation were jointly optimized to yield the minimum total completion time of all tasks. In these works, the data collection phase was often neglected so that the trajectories of the UAVs were either excluded from the optimization or influenced only by the data delivery phase.

In this work, we consider the joint trajectory design and resource allocation of multiple UAVs for tasks that involve both on-demand image capture and wireless delivery to requesting users on the ground. The UAVs are given a number of surveillance tasks for applications, such as traffic monitoring, security surveillance, and search and rescue, where the delivery times of the images are essential. In each task, UAVs are required to capture the image of a specified surveillance region and deliver the image to the requesting user before a specified deadline. The widespread locations of the capture and delivery targets and the heterogeneity of the deadlines make the problem challenging to solve. To solve this problem, we propose a solution in which the task assignment, transmission scheduling, and trajectory designs are jointly determined to maximize the total surveillance area of the completed tasks subject to constraints on the field-of-view of the camera and the transmission resources. The problem is solved for both single-UAV and multiple-UAV scenarios. The main contributions of this work are summarized as follows:

- We propose using UAVs to serve on-demand image surveillance tasks where the UAVs capture the required surveillance regions and then send the image to the requesting user before specific deadlines. These demands may appear in many applications, such as traffic monitoring, border patrol, structural inspection, search and rescue, etc.
- In the single-UAV scenario, we examine the joint design of the UAV's trajectory task assignment and transmission scheduling to maximize the total surveillance area of the completed tasks. A field-of-view coverage constraint is adopted to ensure successful image capture of the surveillance region and an information causality constraint is considered to ensure that the images are captured before they are delivered to the requesting users.
- We propose an alternating optimization algorithm to solve the resulting mixed-integer nonlinear programming (MINLP) problem. We relax the binary constraints on the task assignment and transmission scheduling variables and adopt techniques from the exact penalty method (EPM) to promote near-binary solutions. The nonconvex

trajectory optimization problem is then solved by a successive convex approximation (SCA) approach.

- In the multiple-UAV scenario, we further propose a cooperative image capture and delivery scheme that allows an image to be captured by one UAV and delivered to the requesting user through relaying by another UAV. The problem is particularly challenging since the local solutions at different UAVs are now strongly coupled.
- We propose a distributed implementation that utilizes a set of auxiliary local deadlines to decouple the multiple-UAV problem into multiple single-UAV problems that can be solved in parallel in each iteration.
- Numerical simulations are provided to validate the efficacy of the proposed algorithms. The result shows that our proposed scheme significantly improves upon baseline approaches based on the nearest-distance and nearest-deadline trajectories, the greedy transmission scheduling, and the Sense-and-Send scheme adapted from [10]. In the multiple-UAV case, we can further see the advantage of relaying among UAVs to efficiently cover large network areas.

It is worthwhile to note that most existing works, e.g., [12], [13], [14], [15], and [16], focus only on data collection from IoT devices to the UAV, considering the UAV or a single remote data collection point as the final destination. This is also the case for related works in image surveillance and UAV sensing, as mentioned in [5], [6], [7], [8], [9], [10], and [11]. Our proposed work considers a much more challenging scenario where the images captured at different locations need to be delivered to different users, instead of a single destination. In this case, the image capture and data delivery tasks must be appropriately interleaved, taking into consideration the fact that images must be captured before they can be delivered. Moreover, by considering image capture rather than wireless information transfer, the UAVs must conform to more stringent flight trajectory constraints. To the best of our knowledge, we are the first to examine the UAV-enabled image capture and delivery problem with different destination points. The extension to multiple UAVs is even more challenging since one must further optimize the UAVs' relay decisions as well as the scheduling of relay tasks that are received from other UAVs.

The remainder of this paper is organized as follows. In Section II, we describe the system model and problem formulation for the single-UAV case. In Section III, we propose a solution for the joint task assignment, transmission scheduling, and UAV trajectory design problem. In Section IV, we extend our proposed scheme to the multiple-UAV case, where relaying by neighboring UAVs is considered to serve tasks with widely separated surveillance regions and requesting users. Finally, we present numerical results in Section V and conclude our work in Section VI.

II. System Model and Problem Formulation

Let us first consider the single-UAV scenario, where an image surveillance UAV is utilized for on-demand image capture and delivery services to ground users. The multiple-UAV scenario will be discussed in Section IV. The objective

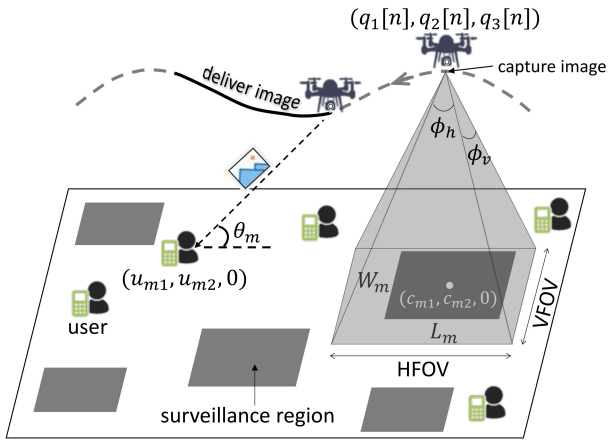

Fig. 1. System model.

is to maximize the total area of completed tasks during each assignment period of N time slots. A set of M tasks, denoted by $\mathcal{M} = \{1, \ldots, M\}$, is received by the UAV prior to the start of each period. For each task, the UAV must capture the image of a specified surveillance region (or target area) on the ground and deliver the image to the requesting user before the deadline, as illustrated in Fig. 1. The above scenario may arise in many different scenarios. For example, in vehicular applications, drivers may be requesting images of traffic conditions ahead or possible collision threats around corners; in city patrol, policemen may be requesting images of traffic accidents or instant crime scenes to enable timely responses; in security applications, fresh images of private homes or secure sites may be requested to identify unauthorized entry; in search-and-rescue missions, the prompt monitoring of disaster areas may also be required. In these scenarios, timely capture of images in the order of seconds or minutes is essential to enable fast and timely responses. The surveillance region of task m lies within a rectangular area of length L_m and width W_m, centered at position $\mathbf{c}_m = (c_{m1}, c_{m2}, 0)$, and the user requesting the image is at position $\mathbf{u}_m = (u_{m1}, u_{m2}, 0)$. The deadline for delivering the image of task m to its requesting user is T_m ($\leq N$).

A. Image Surveillance Model

To accomplish each task, the UAV must first fly to a position that can capture the surveillance region within its field of view and then fly toward the requesting user to facilitate the delivery at a higher transmission rate. Suppose that $\mathbf{q}[n] \triangleq (q_1[n], q_2[n], q_3[n])$, for $n = 1, \ldots, N$, is the position of the UAV at time n, and that ϕ_h and ϕ_v are the horizontal and vertical angles-of-view of the UAV-mounted camera. Then, the horizontal field-of-view (HFOV) and the vertical field-of-view (VFOV) can be computed as $\text{HFOV}[n] = 2q_3[n] \tan \frac{\phi_h}{2}$ and $\text{VFOV}[n] = 2q_3[n] \tan \frac{\phi_v}{2}$ [21], respectively. Hence, the rectangular region covered by the UAV in slot n is given by $[q_1[n] - q_3[n] \tan \frac{\phi_h}{2}, q_1[n] + q_3[n] \tan \frac{\phi_h}{2}] \times [q_2[n] - q_3[n] \tan \frac{\phi_v}{2}, q_2[n] + q_3[n] \tan \frac{\phi_v}{2}]$. For simplicity, we assume that the HFOV and VFOV of the camera can always be aligned to the length and width of the surveillance region.

Let $a_m[n] \in \{0,1\}$ be the binary task assignment variable defined such that $a_m[n]=1$ if the surveillance region of task m is to be captured in slot n and $a_m[n]=0$, otherwise. The assignment of task m over N time slots, i.e., $\{a_m[n]\}_{n=1}^N$, is feasible only if

$$q_1[n]+q_3[n]\tan\frac{\phi_h}{2} \geq c_{m1}+\frac{L_m}{2}-(1-a_m[n])B_{\text{big}}, \quad (1a)$$

$$q_1[n]-q_3[n]\tan\frac{\phi_h}{2} \leq c_{m1}-\frac{L_m}{2}+(1-a_m[n])B_{\text{big}}, \quad (1b)$$

$$q_2[n]+q_3[n]\tan\frac{\phi_v}{2} \geq c_{m2}+\frac{W_m}{2}-(1-a_m[n])B_{\text{big}}, \quad (1c)$$

$$q_2[n]-q_3[n]\tan\frac{\phi_v}{2} \leq c_{m2}-\frac{W_m}{2}+(1-a_m[n])B_{\text{big}}, \quad (1d)$$

where B_{big} is chosen large enough so that the UAV position is unconstrained when $a_m[n]=0$. For example, in the simulations, we choose B_{big} equal to the length of the entire network area. When $a_m[n]=1$, the constraints in (1) ensure that the surveillance region is covered by the field-of-view of the UAV-mounted camera in slot n. Moreover, since each task is served only once, we have $\sum_{n=1}^{T_m} a_m[n] \leq 1$, for all m. In addition, we also impose a constraint on the minimum resolution of the captured image measured in terms of the number of pixels per meter (PPM). In particular, for the image captured in slot n, we define PPM in both the horizontal and vertical directions as $\text{PPM}_h[n] \triangleq \frac{I_h}{\text{HFOV}[n]} = \frac{I_h}{2\tan\frac{\phi_h}{2}q_3[n]}$ and $\text{PPM}_v[n] \triangleq \frac{I_v}{\text{VFOV}[n]} = \frac{I_v}{2\tan\frac{\phi_v}{2}q_3[n]}$, where I_h and I_v are the numbers of pixels in the horizontal and vertical dimensions of the image sensor [21], [22]. By letting η be the minimum required image resolution so that $a_m[n]\eta \leq \min\{\text{PPM}_h[n], \text{PPM}_v[n]\}$, we obtain a constraint on the UAV altitude given by

$$a_m[n]q_3[n] \leq \frac{1}{2\eta}\min\left\{\frac{I_h}{\tan\frac{\phi_h}{2}}, \frac{I_v}{\tan\frac{\phi_v}{2}}\right\}, \quad (2)$$

for all m and n. Each image is downsampled to resolution η and cropped so that only the area of interest is preserved. Hence, to complete the task, the number of bits that must be delivered to the requesting user is $L_m W_m \eta^2 b$, where b is the number of bits used to represent each pixel.

B. Communications Model

Following [23] and [24], we adopt the probabilistic line-of-sight (LoS) channel model to characterize the quality of the UAV to user links. In particular, we assume that the channel between the UAV and user m in slot n is LoS with probability

$$P_m^{\text{LoS}}(\mathbf{q}[n]) = \frac{1}{1+C_1 e^{-C_2\left(\frac{180}{\pi}\sin^{-1}\frac{q_3[n]}{\|\mathbf{q}[n]-\mathbf{u}_m\|}-C_1\right)}}, \quad (3)$$

where $\frac{180}{\pi}\sin^{-1}\frac{q_3[n]}{\|\mathbf{q}[n]-\mathbf{u}_m\|}$ is the elevation angle from user m to the UAV in slot n, and C_1 and C_2 are constant parameters that depend on the environment. In this case, the transmission rate to user m in slot n, i.e., $r_m[n]$, is bounded by the average achievable rate $\bar{R}_m(\mathbf{q}[n]) = P_m^{\text{LoS}}(\mathbf{q}[n])R_m^{\text{LoS}}(\mathbf{q}[n]) + (1-P_m^{\text{LoS}}(\mathbf{q}[n]))R_m^{\text{NLoS}}(\mathbf{q}[n])$, where $R_m^{\text{LoS}}(\mathbf{q}[n])$ and $R_m^{\text{NLoS}}(\mathbf{q}[n])$ are the achievable rates between the UAV and user m under LoS and non-LoS (NLoS) channels, respectively. By assuming that the NLoS rate is negligible compared to the LoS rate, as done in [23] and [24], we can approximate the constraint as

$$r_m[n] \leq \bar{R}_m(\mathbf{q}[n]) \approx P_m^{\text{LoS}}(\mathbf{q}[n])R_m^{\text{LoS}}(\mathbf{q}[n]) \quad (4)$$

where

$$R_m^{\text{LoS}}(\mathbf{q}[n]) = B\log_2\left(1+\frac{P}{\sigma^2\|\mathbf{q}[n]-\mathbf{u}_m\|^\alpha}\right). \quad (5)$$

Here, B is the channel bandwidth, P is the transmit power, α is the path loss exponent under LoS (e.g., $\alpha=2.5$ in [24]), and σ^2 is the receiver noise power.[1]

Let $s_m[n] \in \{0,1\}$ be the binary transmission scheduling variable, where $s_m[n]=1$ if UAV transmits to user m in slot n and $s_m[n]=0$, otherwise. We assume that each slot is scheduled to only one user and, thus, $\sum_{m=1}^M s_m[n] \leq 1$, for all n. To deliver the image to the requesting user before the deadline T_m, we must ensure that the image data size is less than the total number of bits transmitted over the scheduled time slots since the time of image capture, i.e.,

$$\sum_{n=n'}^{T_m} a_m[n]L_m W_m \eta^2 b \leq \sum_{n=n'}^{T_m} s_m[n]r_m[n]\tau \quad (6)$$

for $n'=1,\ldots,T_m$, where τ is the time slot duration. Notice that the left-hand-side (LHS) is equal to $L_m W_m \eta^2 b$, if n' is less than the image capture time, and is 0, otherwise.

C. Problem Formulation

In this work, we aim to jointly determine the UAV trajectory $\{\mathbf{q}[n]\}_{n=1}^N$, the task assignment $\{a_m[n]\}_{n=1}^N$, and transmission scheduling $\{s_m[n]\}_{n=1}^N$, for all m, that maximize the total area of the surveillance regions of the completed tasks. This objective can be viewed as maximizing the sum of weighted tasks served by the UAV with the weight being chosen as the area of the target region. In practice, the weight could also be chosen differently depending on the notion of reward in different applications. The proposed problem can be formulated as

$$\max_{\substack{\mathbf{q}[n],s_m[n],a_m[n],\\ r_m[n],\theta_m[n],\forall m,n}} \sum_{m=1}^M\sum_{n=1}^{T_m} a_m[n]L_m W_m \quad (7a)$$

$$\text{subject to} \quad (1a),\ (1b),\ (1c),\ (1d),\ (2),\ (6) \quad (7b)$$

$$a_m[n]\in\{0,1\},\ s_m[n]\in\{0,1\},\ \forall n,m, \quad (7c)$$

$$r_m[n] \leq \frac{B\log_2\left(1+\frac{P/\sigma^2}{\|\mathbf{q}[n]-\mathbf{u}_m\|^\alpha}\right)}{1+C_1 e^{-C_2(\theta_m[n]-C_1)}}, \forall m,n, \quad (7d)$$

$$\theta_m[n] \leq \frac{180}{\pi}\sin^{-1}\frac{q_3[n]}{\|\mathbf{q}[n]-\mathbf{u}_m\|}, \forall m,n, \quad (7e)$$

[1] In practice, the total noise power may incorporate parameters such as channel bandwidth, noise power spectral density, reference channel power gain, and SNR gap due to practical coding and modulation. However, we do not consider these parameters in the system model for ease of exposition. These parameters will be taken into account when choosing the noise power in our numerical results section.

$$0 \le \theta_m[n] \le 90,\ \forall m, n, \tag{7f}$$
$$\sum_{n=1}^{T_m} a_m[n] \le 1,\ \forall m, \tag{7g}$$
$$\sum_{m=1}^{M} s_m[n] \le 1,\ \forall n, \tag{7h}$$
$$\|\mathbf{q}[n-1] - \mathbf{q}[n]\| \le v_{\max}\tau,\ \forall n \ge 2, \tag{7i}$$
$$h_{\min} \le q_3[n] \le h_{\max},\ \forall n, \tag{7j}$$
$$\mathbf{q}[1] = \mathbf{q}_{\text{start}}. \tag{7k}$$

The constraint in (7d) is obtained by substituting (3) and (5) into (4) and replacing the elevation angle with an auxiliary variable $\theta_m[n]$. Furthermore, $v_{\max}$ is the maximum speed, $h_{\min}$ and $h_{\max}$ are the minimum and maximum altitudes, and $\mathbf{q}_{\text{start}}$ is the start point of the UAV. Here, we assume that the total time duration over N time slots is much shorter than the maximum flight endurance of a typical rotary-wing UAV in the market. Hence, we do not explicitly consider the UAV's energy constraint since it would be inactive under the considered application scenario.

The optimization problem in (7) is a mixed integer nonlinear programming problem (MINLP) that is hard to solve in general. In the following, we propose an alternating optimization solution using successive convex approximation (SCA) and the exact penalty method (EPM).

III. Joint UAV Trajectory, Task Assignment, and Transmission Scheduling Algorithm for the Single-UAV Scenario

In this section, we propose an efficient solution for the joint optimization of the UAV trajectory, task assignment, and transmission scheduling to maximize the total area of completed tasks. To solve the problem, we first relax the binary constraints on the assignment and scheduling variables $a_m[n]$ and $s_m[n]$, for all m and n, and impose a penalty to promote binary solutions, similar to the exact penalty method (EPM) in [25]. By doing so, we obtain the relaxed problem below:

$$\max_{\substack{\mathbf{q}[n], s_m[n], a_m[n], \\ r_m[n], \theta_m[n], v_m[n], \\ \nu_m[n], \forall m, n}} \sum_{m=1}^{M}\sum_{n=1}^{T_m} a_m[n] L_m W_m + \lambda\Bigg[\sum_{m=1}^{M}\sum_{n=1}^{T_m}(2a_m[n]-1)(2v_m[n]-1) + \sum_{m=1}^{M}\sum_{n=1}^{T_m}(2s_m[n]-1)(2\nu_m[n]-1)\Bigg] \tag{8a}$$

subject to
$$0 \le a_m[n] \le 1,\ \forall m, n, \tag{8b}$$
$$0 \le s_m[n] \le 1,\ \forall m, n, \tag{8c}$$
$$\sum_{m=1}^{M}\sum_{n=1}^{T_m}(2v_m[n]-1)^2 \le \sum_{m=1}^{M} T_m, \tag{8d}$$
$$\sum_{m=1}^{M}\sum_{n=1}^{T_m}(2\nu_m[n]-1)^2 \le \sum_{m=1}^{M} T_m, \tag{8e}$$
$$\text{(1a)–(1d), (2), (6), (7d)–(7k)}, \tag{8f}$$

where $v_m[n]$ and $\nu_m[n]$ are auxiliary penalty variables that are used to force the solutions of $a_m[n]$ and $s_m[n]$ close to 0 or 1. The above formulation is justified by the result in [25, Lemma 1] which shows that, if $\mathbf{0} \le \mathbf{a} \le \mathbf{1}$ and $\|2\mathbf{v}-\mathbf{1}\|^2 \le d$, then $(2\mathbf{a}-\mathbf{1})^T(2\mathbf{v}-\mathbf{1}) \le d$ and, if the equality holds, then $\mathbf{a} \in \{0,1\}^d$, $\mathbf{v} \in \{0,1\}^d$ and $\mathbf{a} = \mathbf{v}$, where $\mathbf{0}$ and $\mathbf{1}$ are d-dimensional all-zero and all-one vectors, respectively. In the proposed problem, $v_m[n]$ (or, similarly, $\nu_m[n]$), for all m and n, are the auxiliary penalty variables that form the vector $\mathbf{v}$, in which case, the dimension is given by $d = \sum_{m=1}^{M} T_m$. Hence, by maximizing the penalty term in (8a), the solution for $a_m[n]$ and $v_m[n]$, for all m and n, can be forced close to 0 or 1.

Notice that the problem in (8) is still nonconvex and, thus, is difficult to solve optimally in general. To obtain an efficient solution, we propose an alternating optimization approach where the task assignment and transmission scheduling, the UAV trajectory, and the penalty variables are optimized in turn until convergence. In particular, suppose that $\mathbf{q}^{(t)}[n]$, $s_m^{(t)}[n]$, $a_m^{(t)}[n]$, $r_m^{(t)}[n]$, $\theta_m^{(t)}[n]$, $v_m^{(t)}[n]$, and $\nu_m^{(t)}[n]$ are the solutions obtained at the end of iteration t. Then, the optimization subproblems in iteration $t+1$ can be described as follows.

A. Subproblem I: Task Assignment & Transmission Scheduling

Given the UAV trajectory $\mathbf{q}^{(t)}[n]$, transmission rate $r_m^{(t)}[n]$, elevation angle $\theta_m^{(t)}[n]$, and penalty variables $v_m^{(t)}[n]$ and $\nu_m^{(t)}[n]$ in iteration t, the optimization of the task assignment and transmission scheduling variables (i.e., $a_m[n]$ and $s_m[n]$, $\forall m, n$) can be formulated as

$$\max_{\substack{s_m[n], a_m[n], \\ \forall m, n}} \sum_{m=1}^{M}\sum_{n=1}^{T_m} a_m[n] L_m W_m + \lambda\Gamma(\{a_m[n]\}, \{s_m[n]\}, \{v_m^{(t)}[n]\}, \{\nu_m^{(t)}[n]\}) \tag{9a}$$

subject to (1a)–(1d), (2), (6), (7g), (7h), (8b), (8c), (9b)

where

$$\Gamma(\{a_m[n]\}, \{s_m[n]\}, \{v_m[n]\}, \{\nu_m[n]\}) \triangleq \sum_{m=1}^{M}\sum_{n=1}^{T_m}(2a_m[n]-1)(2v_m[n]-1) + \sum_{m=1}^{M}\sum_{n=1}^{T_m}(2s_m[n]-1)(2\nu_m[n]-1). \tag{10}$$

The problem in (9) is a linear programming problem that can be solved by off-the-shelf solvers such as CVX [26]. The resulting solution is denoted by $\tilde{a}_m^{(t+1)}[n]$ and $s_m^{(t+1)}[n]$, $\forall m, n$.

B. Subproblem II: Task Assignment, UAV Trajectory & Rate Optimization

Given $s_m^{(t+1)}[n]$, $v_m^{(t)}[n]$, and $\nu_m^{(t)}[n]$, the optimization over the task assignment, UAV trajectory, and transmission rates

can be written as

$$\max_{\substack{\mathbf{q}[n],r_m[n],\\ \theta_m[n],a_m[n],\\ \forall m,n}} \sum_{m=1}^{M}\sum_{n=1}^{T_m} a_m[n]L_mW_m + \lambda\Gamma(\{a_m[n]\},\{s_m^{(t+1)}[n]\},\{v_m^{(t)}[n]\},\{\nu_m^{(t)}[n]\}) \tag{11a}$$

$$\text{subject to } (1a)\text{–}(1d),\ (2),\ (6), \tag{11b}$$

$$(7d),\ (7e),\ (7f),\ (7g),\ (7i)\text{–}(7k),\ (8b). \tag{11c}$$

Notice that, even though the task assignment has already been optimized in Subproblem I, we include it again in Subproblem II to enable more flexibility in the trajectory design. However, the above problem is nonconvex due to the constraints in (2), (7d) and (7e). Hence, to obtain a tractable solution, we adopt a successive convex approximation (SCA) approach where the above constraints are replaced with their convex approximations, as described in the following.

First, by rewriting the constraints in (2) as

$$\frac{2\eta a_m[n]}{\min\left\{\frac{I_h}{\tan\frac{\phi_h}{2}},\frac{I_v}{\tan\frac{\phi_v}{2}}\right\}} \le \frac{1}{q_3[n]} \tag{12}$$

and by lower-bounding the right-hand-side (RHS) by its first-order Taylor expansion, we obtain the convex constraint

$$\frac{2\eta a_m[n]}{\min\left\{\frac{I_h}{\tan\frac{\phi_h}{2}},\frac{I_v}{\tan\frac{\phi_v}{2}}\right\}} \le \frac{1}{q_3^{(t)}[n]} - \frac{q_3[n]-q_3^{(t)}[n]}{(q_3^{(t)}[n])^2}. \tag{13}$$

Moreover, by the fact that $\frac{A}{x}\log_2\left(1+\frac{\gamma}{y^{\frac{\alpha}{2}}}\right)$ is convex with respect to x and y, for all $x>0, y>0$, $A\ge 0, \gamma\ge 0$, and $2\le\alpha\le 4$ [23, Lemma 1], we can show that the RHS of the constraint in (7d) is a convex function with respect to $1+e^{-C_2(\theta_m[n]-C_1)}$ and $\|\mathbf{q}[n]-\mathbf{u}_m\|^2$. In this case, the RHS of (7d) can again be lower-bounded by its first-order Taylor expansion as

$$\begin{aligned}&\frac{B\log_2\left(1+\frac{P/\sigma^2}{\|\mathbf{q}[n]-\mathbf{u}_m\|^\alpha}\right)}{1+C_1e^{-C_2(\theta_m^{(t)}[n]-C_1)}}\\ &\ge B\Big[\Omega_{1,m}^{(t)}[n]-\Psi_{1,m}^{(t)}[n]\\ &\quad\times\left(C_1e^{-C_2(\theta_m[n]-C_1)}-C_1e^{-C_2(\theta_m^{(t)}[n]-C_1)}\right)\\ &\quad-\Lambda_{1,m}^{(t)}[n]\left(\|\mathbf{q}[n]-\mathbf{u}_m\|^2-\|\mathbf{q}^{(t)}[n]-\mathbf{u}_m\|^2\right)\Big]\end{aligned} \tag{14}$$

where $\Omega_{1,m}^{(t)}[n] \triangleq \frac{\log_2\left(1+\frac{P/\sigma^2}{(\|\mathbf{q}^{(t)}[n]-\mathbf{u}_m\|^2)^{\alpha/2}}\right)}{1+C_1e^{-C_2(\theta_m^{(t)}[n]-C_1)}}$, $\Psi_{1,m}^{(t)}[n] \triangleq \frac{\log_2\left(1+\frac{P/\sigma^2}{(\|\mathbf{q}^{(t)}[n]-\mathbf{u}_m\|^2)^{\alpha/2}}\right)}{\left(1+C_1e^{-C_2(\theta_m^{(t)}[n]-C_1)}\right)^2}$, and $\Lambda_{1,m}^{(t)}[n] \triangleq \frac{1}{1+C_1e^{-C_2(\theta_m^{(t)}[n]-C_1)}}\cdot\frac{\frac{(\alpha/2)(P/\sigma^2)\log_2 e}{(\|\mathbf{q}^{(t)}[n]-\mathbf{u}_m\|^2)^{(\alpha+2)/2}}}{1+\frac{P/\sigma^2}{(\|\mathbf{q}^{(t)}[n]-\mathbf{u}_m\|^2)^{\alpha/2}}}$. By replacing the RHS of the constraint in (7d) by the lower bound in (14), we obtain an approximate convex constraint

$$\begin{aligned}r_m[n]\le B\Big[&\Omega_{1,m}^{(t)}[n]-\Psi_{1,m}^{(t)}[n]\left(C_1e^{-C_2(\theta_m[n]-C_1)}\right.\\ &\left.-C_1e^{-C_2(\theta_m^{(t)}[n]-C_1)}\right)-\Lambda_{1,m}^{(t)}[n]\left(\|\mathbf{q}[n]-\mathbf{u}_m\|^2\right.\\ &\left.-\|\mathbf{q}^{(t)}[n]-\mathbf{u}_m\|^2\right)\Big].\end{aligned} \tag{15}$$

Moreover, notice that constraint (7e) can be written as

$$\ln\left(\sin\frac{\theta_m[n]\pi}{180}\right)+\ln(\|\mathbf{q}[n]-\mathbf{u}_m\|)\le\ln q_3[n]. \tag{16}$$

Here, the first and second terms on the LHS of (16) are strictly concave concerning $\frac{\theta_m[n]\pi}{180}$ and $\|\mathbf{q}[n]-\mathbf{u}_m\|$, respectively. This is because $\ln(\sin x)$ is strictly concave, for $0<x\le\frac{\pi}{2}$, and $\ln x$ is strictly concave, for $x>0$. By replacing the terms on the LHS of (16) by their respective first-order Taylor expansions, we obtain an approximate convex constraint

$$\begin{aligned}&\Omega_{2,m}^{(t)}[n]+\Psi_{2,m}^{(t)}[n]\left(\frac{\theta_m[n]\pi}{180}-\frac{\theta_m^{(t)}[n]\pi}{180}\right)+\Omega_{3,m}^{(t)}[n]\\ &+\Psi_{3,m}^{(t)}[n]\left(\|\mathbf{q}[n]-\mathbf{u}_m\|-\|\mathbf{q}^{(t)}[n]-\mathbf{u}_m\|\right)\le\ln q_3[n],\end{aligned} \tag{17}$$

where $\Omega_{2,m}^{(t)}[n] \triangleq \ln\left(\sin\frac{\theta_m^{(t)}[n]\pi}{180}\right)$, $\Psi_{2,m}^{(t)}[n] \triangleq \cot\frac{\theta_m^{(t)}[n]\pi}{180}$, $\Omega_{3,m}^{(t)}[n] \triangleq \ln(\|\mathbf{q}^{(t)}[n]-\mathbf{u}_m\|)$, and $\Psi_{3,m}^{(t)}[n] \triangleq \frac{1}{\|\mathbf{q}^{(t)}[n]-\mathbf{u}_m\|}$.

To this end, by replacing (2), (7d) and (7e) with (13), (15) and (17), the problem in (11) can be approximated as

$$\max_{\substack{\mathbf{q}[n],r_m[n],\\ \theta_m[n],a_m[n],\\ \forall m,n}} \sum_{m=1}^{M}\sum_{n=1}^{T_m} a_m[n]L_mW_m + \lambda\Gamma(\{a_m[n]\},\{s_m^{(t+1)}[n]\},\{v_m^{(t)}[n]\},\{\nu_m^{(t)}[n]\}) \tag{18a}$$

$$\text{subject to } (1a)\text{–}(1d),\ (6),\ (7f),\ (7g), \tag{18b}$$

$$(7i)\text{–}(7k),\ (8b),\ (13),\ (15),\ (17). \tag{18c}$$

The above problem is convex and, thus, can be solved by standard convex optimization tools. The resulting solution is denoted by $\mathbf{q}^{(t+1)}[n]$, $r_m^{(t+1)}[n]$, $\theta_m^{(t+1)}[n]$, and $a_m^{(t+1)}[n]$.

C. Subproblem III: Penalty Variables Update

Given the solutions of $\mathbf{q}^{(t+1)}[n]$, $r_m^{(t+1)}[n]$, $\theta_m^{(t+1)}[n]$, $a_m^{(t+1)}[n]$ and $s_m^{(t+1)}[n]$ in the previous subproblems, the penalty variables $v_m[n]$ and $\nu_m[n]$ can be updated by solving the following optimization problem

$$\begin{aligned}\underset{\substack{v_m[n],\nu_m[n],\\ \forall m,n}}{\text{argmax}} \ &\sum_{m=1}^{M}\sum_{n=1}^{T_m}\left(2a_m^{(t+1)}[n]-1\right)\left(2v_m[n]-1\right)\\ &+\sum_{m=1}^{M}\sum_{n=1}^{T_m}\left(2s_m^{(t+1)}[n]-1\right)\left(2\nu_m[n]-1\right)\end{aligned} \tag{19a}$$

$$\text{subject to } (8d),\ (8e). \tag{19b}$$

Notice that $v_m^{(t+1)}[n]$ can take on any feasible solution if $a_m^{(t+1)}[n]=\frac{1}{2}$ for some m and n, and yields the solution $v_m^{(t+1)}[n]=\frac{\sqrt{\sum_{m=1}^{M}T_m}(2a_m^{(t+1)}[n]-1)}{2\sqrt{\sum_{m=1}^{M}\sum_{n=1}^{T_m}(2a_m^{(t+1)}[n]-1)^2}}+\frac{1}{2}$, otherwise [25]. Closed-form solutions of $\nu_m^{(t+1)}[n]$ can be obtained similarly with respect to $s_m^{(t+1)}[n]$.

The proposed algorithm for jointly optimizing the UAV trajectory, task assignment, and transmission scheduling is summarized in Algorithm 1. In our proposed algorithm, the

Algorithm 1 Joint Trajectory Design, Transmission Scheduling, and Task Assignment for the Single-UAV Scenario

1: Initialize trajectory $\mathbf{q}^{(0)}[n]$, penalty variables $v_m^{(0)}[n]$ and $\nu_m^{(0)}[n]$, $\forall m, n$, and penalty parameters $\lambda^{(0)} > 0$, $\lambda_{\max} > 0$, $\sigma > 1$, and $I > 1$.
2: Set $\text{Obj}^{[0]} = 0$, $t = 0$.
3: **repeat**
4: Given $\mathbf{q}^{(t)}[n], \theta_m^{(t)}[n], r_m^{(t)}[n], v_m^{(t)}[n]$, and $\nu_m^{(t)}[n]$, solve the problem of task assignment and transmission scheduling in (9) to obtain $a_m^{(t+1)}[n]$, and $s_m^{(t+1)}[n]$, $\forall m, n$.
5: Given $\mathbf{q}^{(t)}[n]$, $v_m^{(t)}[n]$, $\nu_m^{(t)}[n]$, $a_m^{(t+1)}[n]$, and $s_m^{(t+1)}[n]$, solve the problem of task assignment, UAV trajectory, and rate optimization in (18) to obtain $\mathbf{q}^{(t+1)}[n]$, $a_m^{(t+1)}[n]$, $\theta_m^{(t+1)}[n]$, and $r_m^{(t+1)}[n]$, $\forall m, n$.
6: Given $a_m^{(t+1)}[n]$ and $s_m^{(t+1)}[n]$, solve the problem of the penalty variables update in (19) to obtain $v_m^{(t+1)}[n]$ and $\nu_m^{(t+1)}[n]$, $\forall m, n$.
7: Update $\lambda^{(t+1)} \leftarrow \sigma\lambda^{(t)}$ after every I iterations.
8: Set $t \leftarrow t + 1$.
9: **until** $\frac{|\text{Obj}^{[t]} - \text{Obj}^{[t-1]}|}{|\text{Obj}^{[t-1]}|} < \epsilon$
10: Return the solution as $\mathbf{q}^*[n] = \mathbf{q}^{(t)}[n]$, $\theta_m^*[n] = \theta_m^{(t)}[n]$, $r_m^*[n] = r_m^{(t)}[n]$, $s_m^*[n] = s_m^{(t)}[n]$, $a_m^*[n] = a_m^{(t)}[n]$, $v_m^*[n] = v_m^{(t)}[n]$, and $\nu_m^*[n] = \nu_m^{(t)}[n]$, for all m, n.

optimization subproblems in (9), (18), and (19) are solved in turn until convergence. The penalty parameter λ is initially set as a small value to give more flexibility to the optimization but is gradually increased with the number of iterations until the maximum value $\lambda_{\max}$ is reached. The convergence of the proposed algorithm can then be ensured for $\lambda = \lambda_{\max}$.

Theorem 1: Given $\lambda = \lambda_{\max}$, Algorithm 1 yields a sequence of objective values in (8a) that converges.

Proof: For convenience, let us define the notations $\mathbf{q} \triangleq \{\mathbf{q}[n], \forall n\}$, $s \triangleq \{s_m[n], \forall m, n\}$, $a \triangleq \{a_m[n], \forall m, n\}$, $\theta \triangleq \{\theta_m[n], \forall m, n\}$, $v \triangleq \{v_m[n], \forall m, n\}$, and $\nu \triangleq \{\nu_m[n], \forall m, n\}$. With $\lambda = \lambda_{\max}$, let $J_{\text{I}}^{(t)}$, $J_{\text{II}}^{(t)}$, and $J_{\text{III}}^{(t)}$ be the resulting values of the objective function in (8a) after Subproblems I, II, and III, respectively, in iteration t. Subproblem I updates the task assignment and transmission scheduling variables by maximizing the objective value in (8a) (or its reduced form in (9a)). Hence, with the updated solution $\tilde{a}^{(t+1)} \triangleq \{\tilde{a}_m^{(t+1)}[n], \forall m, n\}$ and $s^{(t+1)}$, it must hold that $J_{\text{I}}^{(t+1)} \geq J_{\text{III}}^{(t)}$. Then, in Subproblem II, the constraints (2), (7d), and (7e) are replaced by their convex approximations in (13), (15), and (17). Since the RHS of (13) is a lower bound of the RHS of (12), any solution that is feasible under (13) must also be feasible under (12). By similar arguments, all solutions that are feasible under (15) and (17) must also be feasible under the original constraints in (7d) and (7e). Hence, the solution of Subproblem II is also a feasible solution of the original problem in (8). Moreover, since all bounds are tight at the points $\mathbf{q}^{(t)}$ and $\theta^{(t)}$, i.e., the solutions obtained in iteration t, these points must also be feasible under the convex approximations in (13), (15), and (17). Therefore, we have $J_{\text{II}}^{(t+1)} \geq J_{\text{I}}^{(t+1)}$. Finally, Subproblem III further updates the variables v and ν by maximizing the objective value. Hence, $J_{\text{III}}^{(t+1)} \geq J_{\text{II}}^{(t+1)}$. By the above, we can conclude that $J_{\text{III}}^{(t+1)} \geq J_{\text{III}}^{(t)}$, which implies that the objective value is monotonically non-decreasing and, thus, converges. □

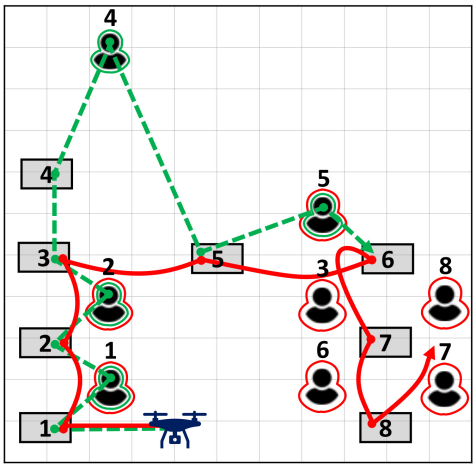

Fig. 2. Illustrative example comparing the proposed and the nearest-distance baseline trajectories in the single-UAV case.

Complexity Analysis: The optimization problems in (9) and (18) are convex and can be solved efficiently by the interior point method supported by several optimization solvers, such as CVX [26]. In this case, solving Subproblem I in (9) requires a complexity of $\mathcal{O}\big((2NM)^3 \ln \frac{1}{\xi}\big)$ [27], where $2NM$ is the number of variables, and $\xi > 0$ indicates the given accuracy. Similarly, solving Subproblem II in (18) requires a complexity of $\mathcal{O}\big((3N + 3NM)^3 \ln \frac{1}{\xi}\big)$. Since Subproblem III provides closed-form solutions, the computational complexity is negligible. Therefore, the proposed algorithm necessitates an overall complexity of $\mathcal{O}\big(\tilde{I}_1[(2NM)^3 + (3N + 3NM)^3] \ln \frac{1}{\xi}\big)$, where $\tilde{I}_1$ is the number of iterations required.

Example: An illustrative example is provided in Fig. 2 to show how the proposed trajectory (represented by the solid red line) may differ from an intuitive nearest-distance baseline trajectory (represented by the dashed green line), which selects the nearest region or user as the next visiting location. We can see that, by jointly optimizing the trajectory and transmission schedule, the proposed trajectory may be bent towards the user receiving the image, instead of moving in a straight line to the next target. Even though the length of the trajectory is slightly increased, the communication rate is improved, resulting in a shorter data transmission time. The proposed optimization exploits this tradeoff to reduce the task completion time and increase the total number of tasks that are served. We can also observe that by neglecting a task that is far away from the main path covering other tasks, more tasks can eventually be served before their respective deadlines. Notice that the nearest-distance baseline instead chooses the nearest task without regard of the locations and deadlines of future tasks. In this case, the UAV may choose to serve task 4, preventing it from serving tasks 6, 7, and 8 before their deadlines. Also, by assuming that the deadline of user 3 is earlier than that of user 5, we can also expect the proposed

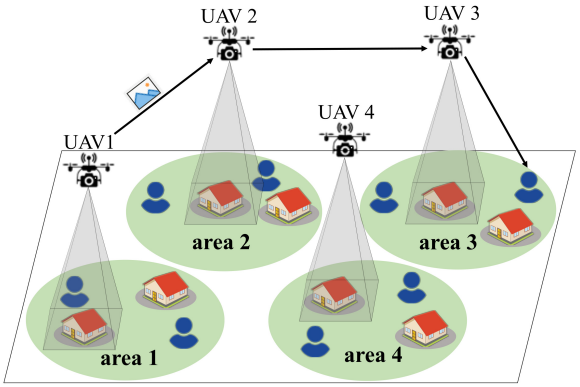

Fig. 3. Illustration of the multiple-UAV scenario where an image of the surveillance region is captured by one UAV and delivered to the requesting user through relaying by other UAVs.

trajectory to bend toward user 3 after visiting region 5 instead of immediately delivering the image of region 5 to its user.

IV. Extension to the Multiple-UAV Scenario With UAV Relaying

In this section, we extend the proposed framework to the case with multiple UAVs that cooperatively serve the on-demand image capture and wireless delivery requests of ground users that are distributed over a wide network area. As the network area increases, the distances between the surveillance regions and the requesting users may become large and, thus, a single-UAV may not be able to reach many regions or users by their deadlines. In this case, the total area of served tasks can be improved significantly by deploying multiple UAVs to cover surveillance regions in different areas and by exploiting cooperation among UAVs to relay the information to the requesting user. Notice that cooperation among UAVs is essential since, otherwise, each UAV may need to fly long distances between surveillance regions and requesting users to complete their assigned tasks, which is extremely time-consuming.

Suppose that the total network area is partitioned into multiple disjoint areas, each served by a different UAV, as shown in Fig. 3. If all users request images only from the coverage areas of their respective UAVs, then the trajectory design, task assignment, and transmission scheduling of different UAVs can be decoupled and solved separately following the single-UAV solution provided in the previous section. However, if a surveillance region and its requesting user fall into different UAVs' coverages, we may have one UAV capture the image and another UAV deliver the information to the requesting user. Other UAVs may serve as dynamic relays in between. In this case, we are interested in determining when and where neighboring UAVs should exchange the message and how the trajectory should be adjusted to accommodate these demands. This introduces a strong dependence among the solutions of different UAVs.

A. System Model and Problem Formulation

Let us consider a system with K UAVs, denoted by the set $\mathcal{K} \triangleq \{1, \ldots, K\}$. The entire network area is partitioned into K disjoint areas $\mathcal{A}^{(1)}, \ldots, \mathcal{A}^{(K)}$, each served by a different UAV. UAV k is responsible for the image capture of task m if the surveillance region is located within the coverage area of UAV k (i.e., if $\mathbf{c}_m \in \mathcal{A}^{(k)}$) and is responsible for the delivery of task m if the requesting user is within its coverage area (i.e., if $\mathbf{u}_m \in \mathcal{A}^{(k)}$). The set of surveillance images and the set of requesting users covered by UAV k are denoted by $\mathcal{M}_{\mathrm{I}}^{(k)}$ and $\mathcal{M}_{\mathrm{U}}^{(k)}$, respectively. Notice that $\mathcal{M}_{\mathrm{I}}^{(k)} \cap \mathcal{M}_{\mathrm{I}}^{(k')} = \emptyset$ and $\mathcal{M}_{\mathrm{U}}^{(k)} \cap \mathcal{M}_{\mathrm{U}}^{(k')} = \emptyset$, for $k \neq k'$, and $\cup_{k=1}^{K} \mathcal{M}_{\mathrm{I}}^{(k)} = \cup_{k=1}^{K} \mathcal{M}_{\mathrm{U}}^{(k)} = \mathcal{M}$. Task m is called a *cross-UAV task* if the image of its surveillance region must be captured by one UAV and delivered by another. For each cross-UAV task, say task m, the relay path from the image capture to delivery is represented by the ordered set of UAVs $\mathcal{P}_m = \{k_{m,1}, \ldots, k_{m,|\mathcal{P}_m|}\}$, where $k_{m,1}$ is the UAV that captures the image and $k_{m,|\mathcal{P}_m|}$ is the UAV delivering the message to user m. Notice that a task $m \in \mathcal{M}_{\mathrm{I}}^{(k)} \cap \mathcal{M}_{\mathrm{U}}^{(k)}$, i.e., a task that does not require cooperation among UAVs, can also be treated as a special case of a cross-UAV task with only a single UAV on the relay path, i.e., $\mathcal{P}_m = \{k\}$. We assume that the relay path can be determined a priori (e.g., by the standard Dijkstra algorithm [28] or by the temporal routing algorithm in [29]), but is not discussed here. The UAVs are assigned orthogonal frequency channels and, thus, can simultaneously transmit to and receive from other UAVs (or users).

Let $\mathbf{q}^{(k)}[n] \triangleq (q_1^{(k)}[n], q_2^{(k)}[n], q_3^{(k)}[n])$ be the position of UAV k in slot n. For task $m \in \mathcal{M}_{\mathrm{I}}^{(k)}$, we can define the binary task assignment variable $a_m^{(k)}[n] \in \{0, 1\}$ such that $a_m^{(k)}[n] = 1$, if the surveillance region of task $m \in \mathcal{M}_{\mathrm{I}}^{(k)}$ is to be captured by UAV k in slot n, and $a_m^{(k)}[n] = 0$, otherwise. Moreover, by extending upon the single-UAV case, we can also define the binary transmission scheduling variable of UAV k as $s_m^{(k)}[n]$ such that $s_m^{(k)}[n] = 1$ if the image of task m is delivered by UAV k in slot n to the next UAV on the relay path or to the requesting user m (if k is the last UAV on the relay path). For $i < |\mathcal{P}_m|$, the inter-UAV transmission rate from UAV $k_{m,i}$ to the next UAV on the path (i.e., $k_{m,i+1}$) in slot n, denoted by $r_m^{(k_{m,i})}[n]$, must satisfy

$$r_m^{(k_{m,i})}[n] \leq B \log_2 \left(1 + \frac{P}{\sigma^2 \|\mathbf{q}^{(k_{m,i})}[n] - \mathbf{q}^{(k_{m,i+1})}[n]\|^{\alpha}}\right). \tag{20}$$

Here, we consider the LoS channel capacity since we assume no obstacle exists in the air-to-air channel. Similarly, the transmission rate $r_m^{(k_{m,|\mathcal{P}_m|})}[n]$ between UAV $k_{m,|\mathcal{P}_m|}$ and user m (i.e., the requesting user of task m) in slot n must satisfy the air-to-ground rate constraints in (4) and (5). Moreover, due to information causality, the inter-UAV transmission rates for UAVs on the relay path $\mathcal{P}_m$ must also satisfy

$$\sum_{n=n'}^{T_m} a_m^{(k_{m,1})}[n] L_m W_m \eta^2 b \leq \sum_{n=n'}^{T_m} s_m^{(k_{m,1})}[n] r_m^{(k_{m,1})}[n] \tau \tag{21}$$

and

$$\sum_{n=n'}^{T_m} s_m^{(k_{m,i-1})}[n] r_m^{(k_{m,i-1})}[n] \tau \leq \sum_{n=n'}^{T_m} s_m^{(k_{m,i})}[n] r_m^{(k_{m,i})}[n] \tau \tag{22}$$

for $i = 2, \ldots, |\mathcal{P}_m|$ and $n' = 1, \ldots, T_m$. For UAV $k_{m,1}$, the task assignment variable $a_m^{(k_{m,1})}[n]$ and trajectory $\mathbf{q}^{(k_{m,1})}[n]$, for all n, must satisfy the image capture constraints in (1) and (2).

Given the above constraints, the joint trajectory design, task assignment, and transmission scheduling problem in the multiple-UAV case can be formulated as follows:

$$\max_{\substack{\mathbf{q}^{(k)}[n],\, s_m^{(k)}[n],\, r_m^{(k)}[n],\\ \theta_m^{(k)}[n],\, \forall n,m,k,\\ a_m^{(k)}[n]\, \forall n, m\in\mathcal{M}_{\mathrm{I}}^{(k)},k}} \sum_{k=1}^{K} \sum_{m\in\mathcal{M}_{\mathrm{I}}^{(k)}} \sum_{n=1}^{T_m} a_m^{(k)}[n] L_m W_m \quad (23a)$$

subject to

$$(1a),\ (1b),\ (1c),\ (1d),\ (2),\ \forall m \in \mathcal{M}_{\mathrm{I}}^{(k)} \text{ and } \forall k, \quad (23b)$$

$$(7d),\ (7e),\ (7f),\ \forall m \in \mathcal{M}_{\mathrm{U}}^{(k)} \text{ and } \forall k, \quad (23c)$$

$$r_m^{(k_{m,i})}[n] \le B \log_2\left(1+\frac{P}{\sigma^2 \|\mathbf{q}^{(k_{m,i})}[n]-\mathbf{q}^{(k_{m,i+1})}[n]\|^{\alpha}}\right), \quad \forall i < |\mathcal{P}_m| \text{ and } \forall m, \quad (23d)$$

$$\sum_{n=n'}^{T_m} a_m^{(k_{m,1})}[n] L_m W_m \eta^2 b \le \sum_{n=n'}^{T_m} s_m^{(k_{m,1})}[n] r_m^{(k_{m,1})}[n]\tau, \quad \forall n', m, \quad (23e)$$

$$\sum_{n=n'}^{T_m} s_m^{(k_{m,i-1})}[n] r_m^{(k_{m,i-1})}[n]\tau \le \sum_{n=n'}^{T_m} s_m^{(k_{m,i})}[n] r_m^{(k_{m,i})}[n]\tau, \quad \forall i > 1, n', m, \quad (23f)$$

$$a_m^{(k)}[n] \in \{0,1\},\ \forall n, m \in \mathcal{M}_{\mathrm{I}}^{(k)}, k, \quad (23g)$$

$$\sum_{n=1}^{T_m} a_m^{(k)}[n] \le 1,\ \forall m \in \mathcal{M}_{\mathrm{I}}^{(k)}, k, \quad (23h)$$

$$s_m^{(k)}[n] \in \{0,1\},\ \forall n, m, k, \quad (23i)$$

$$\sum_{m=1}^{M} s_m^{(k)}[n] \le 1,\ \forall n, k, \quad (23j)$$

$$(7i),\ (7j),\ (7k). \quad (23k)$$

Notice that the multiple-UAV problem described above is significantly more challenging due to the coupling caused by the cross-UAV tasks. Instead of devising an optimal centralized solution, we enable distributed implementation by proposing a heuristic approach to the problem into multiple single-UAV problems with the help of auxiliary deadlines and task assignment variables. In this case, the trajectory and transmission scheduling designs at the different UAVs can be solved in parallel by leveraging the solutions derived in the previous section. The auxiliary variables can then be updated iteratively to improve the effectiveness through collaboration.

B. Proposed Decentralized Solution for the Multiple-UAV Problem

To decouple the multiple-UAV problem into parallel single-UAV problems, we first introduce the auxiliary deadlines $t_{m,1}, t_{m,2}, \ldots, t_{m,|\mathcal{P}_m|}$ for each cross-UAV task m such that $t_{m,1} \le t_{m,2} \le \ldots \le t_{m,|\mathcal{P}_m|} = T_m$. The auxiliary deadline $t_{m,i}$ represents the time by which the transmission from UAV $k_{m,i}$ to the next UAV on the relay path $\mathcal{P}_m$ (i.e., UAV $k_{m,i+1}$) must be completed. Given that UAV $k_{m,i}$ successfully receives the image from its preceding UAV $k_{m,i-1}$ by the deadline $t_{m,i-1}$, we can view $t_{m,i-1}+1$ as the time slot that the image is effectively "captured" by UAV $k_{m,i}$. In this case, we can define the task assignment variable for UAV $k_{m,i}$, for $i > 1$, such that $a_m^{(k_{m,i})}[t_{m,i-1}+1] = 1$, if UAV $k_{m,i}$ chooses to serve task m, and $a_m^{(k_{m,i})}[t_{m,i-1}+1] = 0$, otherwise. Since it is not necessary to consider any other capture time for an intermediate UAV $k_{m,i}$, where $i > 1$, we shall omit the time index of the assignment variable for intermediate UAVs, i.e., let $a_m^{(k_{m,i})} \triangleq a_m^{(k_{m,i})}[t_{m,i-1}+1]$, for all $i > 1$. Notice that a task can be assigned to an intermediate UAV only if all UAVs preceding it can successfully receive the image and pass it on to the next UAV. This is denoted by the indicator $\mu_m^{(k_{m,i})} \in \{0,1\}$, defined such that $\mu_m^{(k_{m,i})} = 1$ if $L_m W_m \eta^2 b \le \sum_{n=t_{m,i'-1}+1}^{t_{m,i'}} s_m^{(k_{m,i'})}[n] r_m^{(k_{m,i'})}[n]\tau$, for all $i' < i$, and $\mu_m^{(k_{m,i})} = 0$, otherwise. Then, given the auxiliary deadlines $t_{m,1}, t_{m,2}, \ldots, t_{m,|\mathcal{P}_m|}$ and by assuming that we can obtain the trajectories of neighboring UAVs and the indicator values $\mu_m^{(k_{m,i})}$, for all m and i, the local trajectory design, task assignment, and transmission scheduling of UAV k can be determined by solving the following single-UAV problem:

$$\max_{\substack{\mathbf{q}^{(k)}[n],\, s_m^{(k)}[n],\, r_m^{(k)}[n],\\ \theta_m^{(k)}[n],\, \forall m,n,\\ a_m^{(k)}[n], \forall m\in\mathcal{M}_{\mathrm{I}}^{(k)}, \forall n,\\ a_m^{(k)}, \forall m\notin\mathcal{M}_{\mathrm{I}}^{(k)}}} \sum_{m\in\mathcal{M}_{\mathrm{I}}^{(k)}} \sum_{n=1}^{t_{m,1}} a_m^{(k)}[n] L_m W_m + \sum_{m\notin\mathcal{M}_{\mathrm{I}}^{(k)}} a_m^{(k)} \mu_m^{(k)} L_m W_m \quad (24a)$$

subject to

$$(1a),\ (1b),\ (1c),\ (1d),\ (2),\ \forall m \in \mathcal{M}_{\mathrm{I}}^{(k)}, \quad (24b)$$

$$(7d),\ (7e),\ (7f),\ \forall m \in \mathcal{M}_{\mathrm{U}}^{(k)}, \quad (24c)$$

$$r_m^{(k)}[n] \le B \log_2\left(1+\frac{P}{\sigma^2 \|\mathbf{q}^{(k_{m,i})}[n]-\mathbf{q}^{(k_{m,i+1})}[n]\|^{\alpha}}\right), \quad \forall m \text{ such that } k = k_{m,i} \text{ for some } i < |\mathcal{P}_m|, \quad (24d)$$

$$\sum_{n=n'}^{t_{m,1}} a_m^{(k)}[n] L_m W_m \eta^2 b \le \sum_{n=n'}^{t_{m,1}} s_m^{(k)}[n] r_m^{(k)}[n]\tau, \quad \forall m \in \mathcal{M}_{\mathrm{I}}^{(k)}, \quad (24e)$$

$$a_m^{(k)} \mu_m^{(k)} L_m W_m \eta^2 b \le \sum_{n=t_{m,i-1}+1}^{t_{m,i}} s_m^{(k)}[n] r_m^{(k)}[n]\tau, \quad \forall m \notin \mathcal{M}_{\mathrm{I}}^{(k)} \text{ such that } k = k_{m,i} \text{ for some } i > 1, \quad (24f)$$

$$\sum_{n=1}^{t_{m,1}} a_m^{(k)}[n] \le 1,\ \forall m \in \mathcal{M}_{\mathrm{I}}^{(k)}, \quad (24g)$$

$$a_m^{(k)} \in \{0,1\},\ \forall m \notin \mathcal{M}_{\mathrm{I}}^{(k)}, \quad (24h)$$

$$(7i),\ (7j),\ (7k),\ (23g),\ (23i),\ (23j). \quad (24i)$$

In the above problem for UAV k, we assumed that the auxiliary deadlines $t_{m,1}, t_{m,2}, \ldots, t_{m,|\mathcal{P}_m|}$ for all tasks are given a priori and the trajectories of neighboring UAVs are known and fixed. However, the choice of the auxiliary deadlines may impact the successful delivery of the images over the relay path

and the trajectories of neighboring UAVs may not remain fixed if they are updated in parallel. Hence, we propose an iterative procedure below that gradually updates the deadlines and trajectories until no further increase can be observed in the objective function.

Specifically, let $\{\mathbf{q}^{(k)[c-1]}[n]\}_{n=1}^{N}$ be the trajectory of UAV k obtained at the end of iteration $c-1$ and $\{s_m^{(k)[c-1]}[n]\}_{n=1}^{N}$ be the corresponding transmission scheduling solution. In iteration c, UAV k updates its local trajectory, task assignment, and transmission scheduling based on knowledge of $\{\mathbf{q}^{(k')[c-1]}[n]\}_{n=1}^{N}$ and $\{s_m^{(k')[c-1]}[n]\}_{n=1}^{N}$ for all k' that is a neighboring UAV of UAV k. In this case, UAV k should schedule transmissions to UAV k' only during time slots for which its trajectory is close to that of UAV k' (or should adjust its trajectory to do so). In addition, UAV k should not deviate significantly from its previous trajectory $\mathbf{q}^{(k)[c-1]}[n]$ during time slots for which it may be receiving data from an upstream UAV since its upstream UAV will not be aware of these changes until the next iteration. In particular, by letting $\mathcal{N}^{(k)[c-1]} \triangleq \{n : s_m^{(k')[c-1]}[n] > 0,$ for k' that precedes k in $\mathcal{P}_m$ for some $m\}$ be the set of time slots in which UAV k is receiving information from its upstream neighbors in iteration $c-1$, we regularize the update of UAV k's trajectory by imposing the penalty term $\lambda_q \sum_{n\in\mathcal{N}^{(k)[c-1]}} \|\mathbf{q}^{(k)}[n]-\mathbf{q}^{(k)[c-1]}[n]\|^2$. Then, by choosing $t_{m,1}^{[c]}, t_{m,2}^{[c]}, \ldots, t_{m,|\mathcal{P}_m|}^{[c]}$ to be the auxiliary deadlines of iteration c, the single-UAV problem at UAV k in iteration c can be formulated as follows:

$$\max_{\substack{\mathbf{q}^{(k)}[n],\, s_m^{(k)}[n],\, r_m^{(k)}[n],\\ \theta_m^{(k)}[n],\,\forall m,n,\\ a_m^{(k)}[n],\forall m\in\mathcal{M}_{\mathrm{I}}^{(k)},\forall n,\\ a_m^{(k)},\forall m\notin\mathcal{M}_{\mathrm{I}}^{(k)}}} \sum_{m\in\mathcal{M}_{\mathrm{I}}^{(k)}} \sum_{n=1}^{t_{m,1}^{[c]}} a_m^{(k)}[n] L_m W_m + \sum_{m\notin\mathcal{M}_{\mathrm{I}}^{(k)}} a_m^{(k)} \mu_m^{(k)[c]} L_m W_m - \lambda_q \sum_{n\in\mathcal{N}^{(k)[c-1]}} \|\mathbf{q}^{(k)}[n]-\mathbf{q}^{(k)[c-1]}[n]\|^2 \tag{25a}$$

subject to

$$(1a),\ (1b),\ (1c),\ (1d),\ (2),\ \forall m\in\mathcal{M}_{\mathrm{I}}^{(k)}, \tag{25b}$$

$$(7d),\ (7e),\ (7f),\ \forall m\in\mathcal{M}_{\mathrm{U}}^{(k)}, \tag{25c}$$

$$r_m^{(k)}[n] \le B\log_2\left(1+\frac{P}{\sigma^2\|\mathbf{q}^{(k_{m,i})}[n]-\mathbf{q}^{(k_{m,i+1})[c-1]}[n]\|^{\alpha}}\right),\quad \forall m \text{ such that } k=k_{m,i} \text{ for some } i<|\mathcal{P}_m|, \tag{25d}$$

$$(7i),\ (7j),\ (7k),\ (23g),\ (23i),\ (23j),\ (24e),\ (24f),\ (24g),\ (24h) \tag{25e}$$

$$\text{with } t_{m,1}^{[c]}, t_{m,2}^{[c]}, \ldots, t_{m,|\mathcal{P}_m|}^{[c]}, \mu_m^{(k)[c]}, \forall m. \tag{25f}$$

Notice that, in (25d), we have replaced the trajectory of neighboring UAVs with that obtained in the previous iteration. Moreover, instead of adopting the binary indicator $\mu_m^{(k)} \in \{0,1\}$, we utilized a soft indicator $\mu_m^{(k)[c]}$ that is chosen as the fraction of the image that UAV k has received from its upstream UAV based on the solution obtained in the previous iteration. That is, for $k=k_{m,i}$, we set $\mu_m^{(k)[c]} \triangleq \min\left\{\sum_{n=t_{m,i-2}^{[c-1]}+1}^{t_{m,i-1}^{[c-1]}} s_m^{(k_{m,i-1})[c-1]}[n] r_m^{(k_{m,i-1})[c-1]}[n]\tau/(L_m W_m \eta^2 b), 1\right\}$. By doing so, UAV k will be more likely to allocate resources to the relaying of task m's image if the image is more successfully received by UAV k from its upstream UAV, and vice versa. In each iteration, the single-UAV problem is solved following the procedures in Section III.

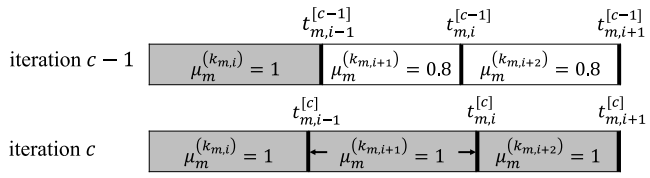

Fig. 4. An example of adjusting time allocation to UAVs over iterations.

Furthermore, notice that the above problem is solved for a given set of auxiliary deadlines $t_{m,1}^{[c]}, t_{m,2}^{[c]}, \ldots, t_{m,|\mathcal{P}_m|}^{[c]}$, for all m. However, the choice of the auxiliary deadlines will affect whether or not all UAVs on the relay path can complete their local relay tasks (i.e., successfully transmitting the received image to the next UAV in time). Therefore, it is necessary to gradually adjust the auxiliary variables to maximize the chance that all UAVs on the relay path are able to complete their local relay tasks. To do so, we propose a heuristic approach based on the evaluation of the completion ratio $\mu_m^{(k)[c]}$ in each iteration. In particular, if the completion ratio is $\mu_m^{(k_{m,i+1})[c]}=1$ for UAV $k_{m,i+1}$ on the relay path of task m, we can infer that UAV $k_{m,i}$ was given sufficient resources to relay the image to UAV $k_{m,i+1}$ during the time frame $t_{m,i-1}^{[c-1]}$ to $t_{m,i}^{[c-1]}$ given in the previous iteration. In this case, the duration previously given to UAV $k_{m,i}$ for the relaying of task m's image, i.e., $t_{m,i-1}^{[c-1]}$ to $t_{m,i}^{[c-1]}$, can be reduced to leave more time for other UAVs on the relay path to complete their local relay tasks. On the other hand, if $\mu_m^{(k_{m,i+1})[c]}<1$, then the duration should be increased instead. Task m is said to be incomplete after iteration c if $\sum_{i\in\mathcal{P}_m}\mu_m^{(k_{m,i})[c]}/|\mathcal{P}_m|<1$, i.e., if it is not completed by all UAVs on the relay path. To enable distributed implementation, we allow all UAVs to update their local deadlines simultaneously based on their respective local completion ratios. That is, for UAV $k_{m,i}$, we let

$$t_{m,i}^{[c]} \leftarrow \begin{cases} t_{m,i}^{[c-1]} - \delta(t_{m,i}^{[c-1]} - t_{m,i-1}^{[c-1]}), & \text{if } \mu_m^{(k_{m,i+1})[c]}=1, \\ t_{m,i}^{[c-1]} + \delta(t_{m,i+1}^{[c-1]} - t_{m,i}^{[c-1]}), & \text{if } \mu_m^{(k_{m,i+1})[c]}<1, \end{cases} \tag{26}$$

where $\delta<1$ represents the percentage of the time duration adjusted in each update. In our experiments, we update the deadlines once every I' iterations to avoid rapid fluctuation. For example, in Fig. 4, we consider the case where the image delivery of task m is complete at UAV $k_{m,i-1}$, i.e., $\mu_m^{k_{m,i}[c-1]}=1$, but is incomplete at UAVs $k_{m,i}$ and $k_{m,i+1}$, e.g., $\mu_m^{k_{m,i+1}[c-1]}<1$ and $\mu_m^{k_{m,i+2}[c-1]}<1$, in iteration $c-1$. In this case, we reduce the time frame of task m at UAV $k_{m,i-1}$ and extend that at UAV $k_{m,i}$, giving more time for UAV $k_{m,i}$ to complete task m in iteration c. Note that a UAV may not be able to achieve a completion ratio of 1 either

Algorithm 2 Distributed Joint Trajectory Design, Transmission Scheduling, and Task Assignment for the Multiple-UAV Scenario

1: Initialize trajectories, $\mathbf{q}^{(k)[0]}[n]$, auxiliary deadlines $t_{m,i}^{[0]}$, completion ratios $\mu_m^{(k_{m,i})[0]}$, $\forall k, m$, and $I' \geq 1$.
2: Set $c = 1$.
3: **repeat**
4: Given $t_{m,i}^{[c-1]}$, $\mathbf{q}^{(k)[c-1]}[n]$, and $\mu_m^{(k_{m,i})[c-1]}$, for all k, m, solve the single-UAV problem of UAV k in (25) for all k to obtain $\mathbf{q}^{(k)[c]}[n]$, $s_m^{(k_{m,i})[c]}[n]$, and $a_m^{(k_{m,i})[c]}[n]$, $\forall k, n, m$.
5: Update $\mu_m^{(k_{m,i})[c]} \leftarrow \min\{\sum_{n=t_{m,i-2}^{[c]}+1}^{t_{m,i-1}^{[c]}} s_m^{(k_{m,i-1})[c]}[n] r_m^{(k_{m,i-1})[c]}[n]\tau/(L_m W_m \eta^2 b), 1\}$.
6: Update the set of incomplete tasks as $\hat{\mathcal{M}}^{[c]} \leftarrow \{m : \sum_{i\in\mathcal{P}_m} \mu_m^{(k_{m,i})[c]}/|\mathcal{P}_m| < 1\}$.
7: For every I' iterations, update the deadlines $t_{m,i}^{[c]}$ by (26), $\forall k$ and $\forall m \in \hat{\mathcal{M}}^{[c]}$.
8: For every $I''(> I')$ iterations, update the set of remaining tasks $\mathcal{M} \leftarrow \mathcal{M} \setminus \{m'\}$, where $m' = \text{argmin}_{m\in\hat{\mathcal{M}}^{[c]}} \sum_{i\in\mathcal{P}_m} \mu_m^{(k_{m,i})[c]}/|\mathcal{P}_m|$.
9: Update $\mathcal{N}^{(k)[c]} \leftarrow \{n : s_m^{(k')[c]}[n] > 0$, for k' that precedes k in $\mathcal{P}_m$ for some $m\}, \forall k$.
10: Set $c - 1 \leftarrow c$.
11: **until** $\{m'\} = \emptyset$

due to limitations of the transmission time frame or because upstream UAVs were not able to fully acquire the image (i.e., the completion ratios of upstream UAVs were already less than 1).

Finally, we further remove a task from the set $\mathcal{M}$ every $I''(> I')$ iterations if it is not able to be completed by all UAVs on the path. By doing so, transmission resources at certain UAVs can be released and reassigned to other tasks. In particular, for every I'' iterations, we remove the task m' that yields the minimum average completion ratio over all UAVs on its path, i.e., $m' = \text{argmin}_m \sum_{i\in\mathcal{P}_m} \mu_m^{(k_{m,i})[c]}/|\mathcal{P}_m|$. The above process is repeated until no incomplete tasks remain. The proposed solution for the multiple-UAV case is summarized in Algorithm 2. It is worthwhile to note that, in the proposed solution, the local single-UAV problem at UAV k can be solved with only knowledge of the trajectory $\{\mathbf{q}^{(k')[c-1]}[n]\}_{n=1}^N$, transmission scheduling $\{s^{(k')[c-1]}[n]\}_{n=1}^N$, and auxiliary deadlines of its neighboring UAVs, e.g., UAV k', in each iteration. The complexity of Algorithm 2 is determined by the complexity of the single-UAV algorithm in Section III since single-UAV problems are solved in parallel in each iteration.

Example: To demonstrate the advantage of cooperation in the multiple-UAV case, we provide an illustrative example with two UAVs each covering a different area as shown in Fig. 5. For cross-UAV tasks (e.g., tasks 1 and 8), the collected images are exchanged with other UAVs when they arrive close to each other. Once images are successfully exchanged, their delivery can be treated as regular local tasks and can be scheduled accordingly. For example, suppose that UAV 1 must deliver region 1's image to its user on the other side, and assume that the two UAVs are 300 meters apart when exchanging data and that the image size is 20 Mbits. Following the inter-UAV transmission rate defined in (20) and the channel parameters in Section V, it can be computed that UAV 1 needs 13 time slots to complete data transmission to UAV 2 when the transmit SNR is 65 dB. The image data can then be delivered along the main path of UAV 2 without requiring a significant detour by the UAV. To serve task 1 without cooperation, UAV 1 must fly toward user 1 and back while delivering the image data directly to the user along the way. Under the considered set of parameters, this may occupy 174 time slots due to the increased flight time and the reduced probability of LoS caused by a smaller elevation angle between the user and the UAV. The inter-UAV transmission time can be considerably reduced to only 4 time slots when the transmit SNR is increased to 80 dB and, thus, cooperation opportunities are expected to increase as the SNR increases.

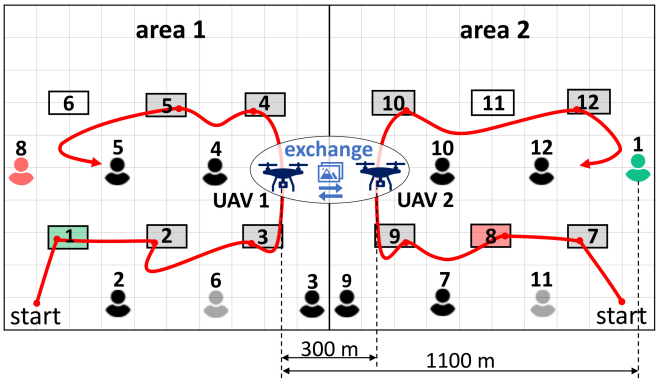

Fig. 5. Illustrative example of image delivery using multiple UAVs working in cooperation.

V. Numerical Results

In this section, we present numerical simulations to demonstrate the effectiveness of our proposed solution. The results are presented separately for the single-UAV and the multiple-UAV scenarios in the following subsections.

A. Results for the Single-UAV Case

In the single-UAV scenario, we assume the surveillance regions and requesting users are randomly deployed according to a uniform distribution in a $[0, 1500] \times [0, 1500]$ m^2 region. The start point of the UAV, i.e., $\mathbf{q}_{\text{start}}$, is uniformly distributed within the region. The number of tasks is $M = 20$, the number of time slots is $N = 400$, and the time slot duration is $\tau = 0.5$ s. The width W_m and the length L_m are uniformly distributed in the intervals $[100, 150]$ and $[W_m, 1.5W_m]$, respectively. The deadline T_m is also chosen randomly with equal probability between 220 and 400 (i.e., N). Unless mentioned otherwise, the UAV's maximum flight speed, minimum height, maximum height, and transmit power are set as $v_{\max} = 20$ m/s, $h_{\min} = 100$ meter, $h_{\max} = 250$ meter, and $P = 32$ dBm, respectively. Following [23]

and [24], we configure the communication channel with bandwidth $B = 2$ MHz, $C_1 = 12$, $C_2 = 0.11$, $\alpha = 2.5$, and total noise power $\sigma^2 = -43$ dBm. The value of σ^2 is obtained by incorporating a noise power spectral density $N_0 = -174$ dBm/Hz along with the channel power gain $\beta_0 = -60$ dB at reference distance $d_0 = 1$ m and a signal-to-noise ratio (SNR) gap $\lambda = 8.2$ dB that accounts for the loss due to practical coding and modulation [23]. The camera specifications are chosen according to [30], where the horizontal and vertical angles of view are $\phi_h = 73.7$ and $\phi_v = 53.1$ degrees, respectively, and the numbers of pixels in the corresponding dimensions are $I_h = 8192$ and $I_v = 5460$, respectively. The minimum required pixel density is $\eta = 25$ [31]. Furthermore, by encoding each pixel using 24 bits and adopting a compression ratio of $\rho = 0.1$, the number of information bits per pixel is given by $b = 24\rho = 2.4$ bits.

We implement five baseline schemes for performance comparison, namely, the proposed trajectory with greedy scheduling (Proposed Traj.+Greedy Sched.), the nearest-distance trajectory with proposed scheduling (ND Traj.+Proposed Sched.), the nearest-distance trajectory with greedy scheduling (ND Traj.+Greedy Sched.), the nearest-deadline trajectory with proposed scheduling (NL Traj.+Proposed Sched.), and the Sense-and-Send scheme [10]. Recall that the UAV's operation involves two actions: image capture and image delivery. The nearest-distance trajectory scheme determines the next action by comparing the distances from the UAV to the uncaptured regions and the requesting users of captured images. If the UAV is closer to an uncaptured region, it will fly to the nearest location that is able to capture the image. If the UAV is closer to a requesting user of a captured image, it will fly toward the user while transmitting data along the way. Once the image delivery is complete, the UAV will stop and seek the next action. The nearest-deadline trajectory scheme, on the other hand, chooses the next action to be either the image capture or image delivery of the task with the closest deadline. To limit the travel distance to the next action, we restrict the initial distance of the next action to be at most 250 meters from the current position of the UAV. The greedy scheduling allocates each time slot to the required delivery with the largest transmission rate. Moreover, we also adapt the Sense-and-Send protocol proposed in [10] to the problem at hand. Here, the UAV performs tasks sequentially in an order given by the nearest-distance policy. After the region of task m is captured, the UAV moves to the region of the next task (i.e., the nearest task) if it is able to complete the data transmission to user m on the way. Otherwise, the UAV flies in the direction of the gradient $\left(\frac{\partial R_m[n]}{\partial q_1[n]}, \frac{\partial R_m[n]}{\partial q_2[n]}, \frac{\partial R_m[n]}{\partial q_3[n]}\right)$ to enhance the transmission rate. In this case, the UAV turns to the direction of the next region once the data transmission to user m is complete. Note that the sensing locations are set as the nearest locations for which the UAV's camera field-of-view can entirely cover the target regions. The speed of the UAV is fixed to $v_{\max}$ in all baseline schemes. Notice that flying at maximum speed $v_{\max}$ may be considered the best greedy approach that favors the next selected task. The nearest-distance trajectory is also employed as the initial solution for our proposed scheme. The simulation results shown in this section are averaged over 200 network realizations.

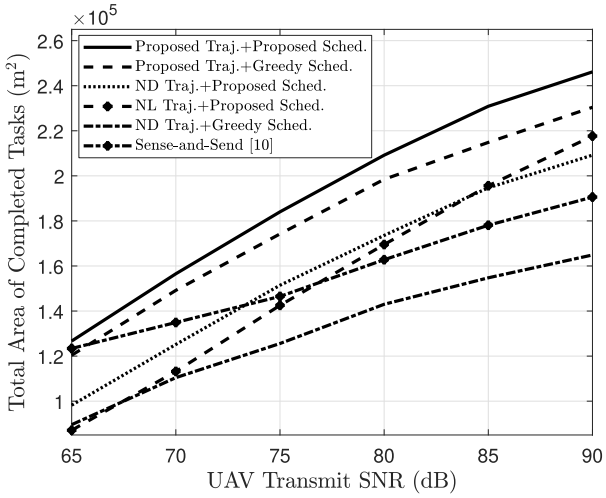

Fig. 6. Total area of completed tasks versus the transmit SNR.

In Fig. 6, we show the total area of completed tasks with respect to the UAV's transmit SNR P/σ^2. We can see that the total area of completed tasks increases with the transmit SNR in all cases and that the proposed trajectory and transmission scheduling schemes outperform all baseline schemes. This is expected since the ND and NL trajectories are not capable of considering the impact of recent trajectory decisions on future assignments and schedules. The ND trajectory may capture more images but may not be able to deliver them in time, whereas the NL trajectory may serve more tasks in a timely manner but may travel longer distances to do so. Moreover, the proposed transmission scheduling scheme is able to schedule image deliveries in accordance with the users' deadlines, which is not considered in the greedy scheduling policy. On the other hand, the Sense-and-Send scheme adopts a sequential task-serving policy, which may overlook the potential of capturing nearby regions first before delivering data from a previous task. Once the delivery of the most recent task is complete, the UAV turns to capture the next region without further utilizing the communication channel. This results in an inefficient use of communication resources.

In Fig. 7, we show the total area of completed tasks with respect to the number of tasks M. The proposed scheme again achieves a better performance than all baseline schemes. As M increases, the UAV will have more tasks to select from, and the distance between surveillance regions and requesting users will also be reduced. In this case, more tasks can be served if the image capture and image delivery actions are scheduled appropriately as done by the proposed scheme. The ND/NL trajectory and greedy scheduling schemes, however, are not able to allocate optimally the time and communication resources to complete both capture and delivery actions of selected tasks. That is, the UAV may sometimes spend more time capturing images, but not enough time delivering the images to the requesting users before their deadlines. Conversely, the Sense-and-Send [10] scheme serves tasks

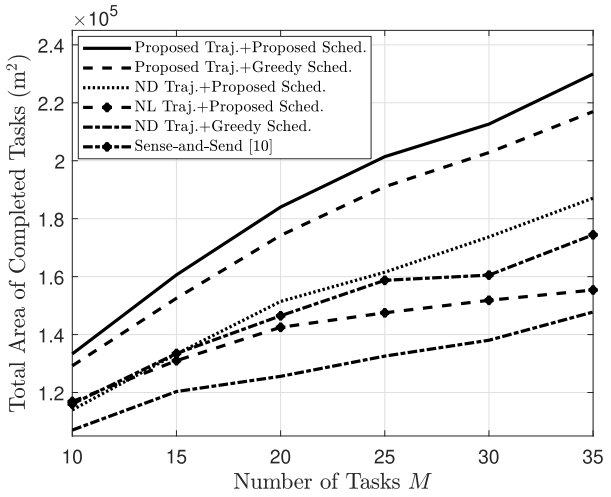

Fig. 7. Total area of completed tasks versus the number of tasks.

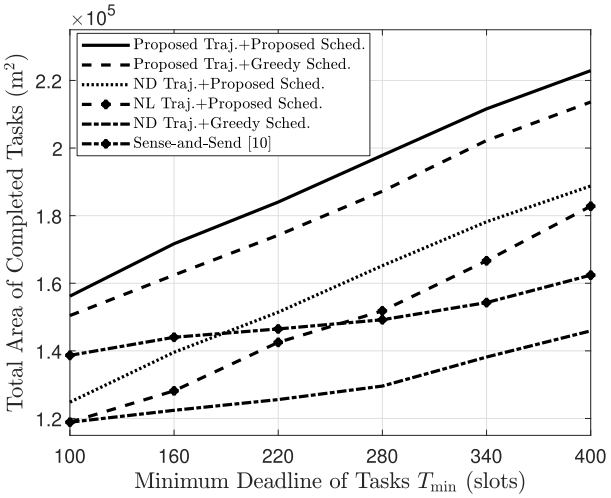

Fig. 8. Total area of completed tasks versus the minimum deadline.

one-by-one (i.e., each region must be captured and delivered before moving on to the next task). Hence, it may ignore the possibility of capturing multiple images in the vicinity of each other before starting to deliver data to their respective users.

In Fig. 8, we examine the performance with respect to the minimum deadline $T_{\min}$, which represents the smallest deadline possible for all tasks. Given $T_{\min}$, each task is assigned a deadline that is chosen randomly according to a uniform distribution between $T_{\min}$ and N. A larger $T_{\min}$ results in longer task deadlines. We can see that the total area of completed tasks increases with $T_{\min}$ in all cases since the UAV is given more time to complete the tasks. The improvement is observed in all cases, but the rate of increase is slower for the baseline that uses neither the proposed trajectory nor the proposed scheduling, i.e., the ND Traj.+Greedy Sched. and the Sense-and-Send [10] scheme.

In Fig. 9, we show a realization of the surveillance regions, requesting users, and the resulting UAV trajectory of the proposed scheme. The UAV captures images of surveillance regions at locations where the field-of-views of the camera can entirely cover the targets, and the captured images can satisfy

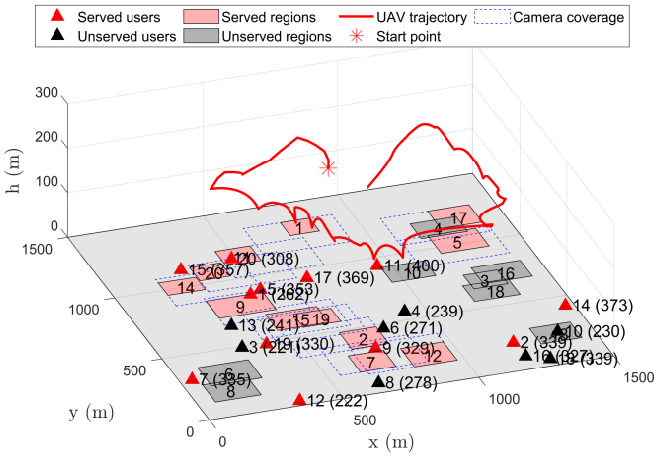

Fig. 9. Example of the surveillance regions, requesting users (with deadlines noted in brackets), and the resulting UAV trajectory of the proposed scheme.

the resolution requirement. When the UAV is traveling from one surveillance region to another, it tends to fly at a higher altitude to increase the probability of experiencing LoS links so that wireless delivery to ground users can be done more efficiently. Moreover, we can see that, under strict deadline constraints, the UAV tends to traverse areas with more or larger surveillance regions. Regions that are far away from the main path are often neglected.

B. Results for the Multiple-UAV Case

In the multiple-UAV scenario, we assume that $K = 6$ UAVs are dispatched to cover a $[0, 4500] \times [0, 3000]$ m^2 area. The surveillance regions and requesting users are uniformly distributed within this area. The entire network area is divided equally into 6 disjoint coverage areas $\mathcal{A}_1$, $\mathcal{A}_2$, ..., $\mathcal{A}_6$, each with 1500×1500 m^2. The start points of the UAVs are randomly placed in their respective coverage areas, and the number of tasks is $M = 40$. All other parameters are set as in the single-UAV case. We compare the proposed scheme with five baseline schemes in the multiple UAV case, including the Proposed Traj.+Greedy Sched. and the ND Traj.+Proposed Sched. schemes (similar to those in the single-UAV case) and three other schemes that do not utilize relaying between UAVs. Similar to the single-UAV case, ND Traj. determines the next action by comparing the distances from the UAV to the uncaptured regions and requesting users. Here, the requesting users may also be neighboring UAVs on the relay path. Greedy Sched. again allocates each time slot to the requesting user or neighboring UAV with the largest transmission rate. Since both schemes require knowledge of neighboring UAVs' locations, we also adopt an iterative procedure where the decisions in each iteration are made based on the neighboring UAVs' locations in the previous iteration. In the non-relaying schemes, we assume that each UAV is responsible for both capturing and delivering the images of its assigned tasks without relaying by other UAVs. In this case, the task assignment, trajectory design, and transmission scheduling can be viewed as single-UAV problems and, thus, can be solved separately by each UAV. The two non-relaying

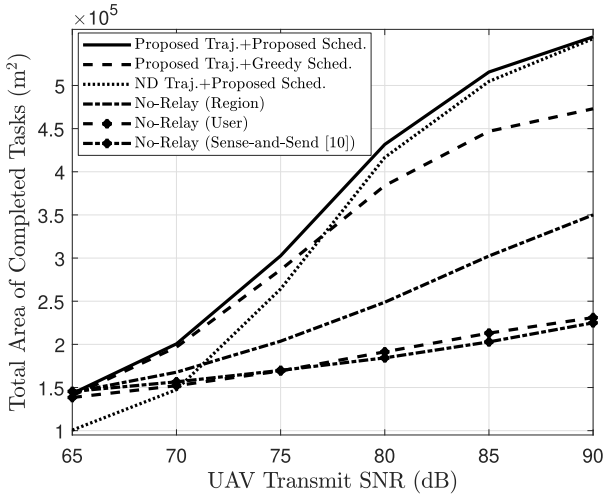

Fig. 10. Total area of completed tasks versus the transmit SNR in the multiple-UAV case.

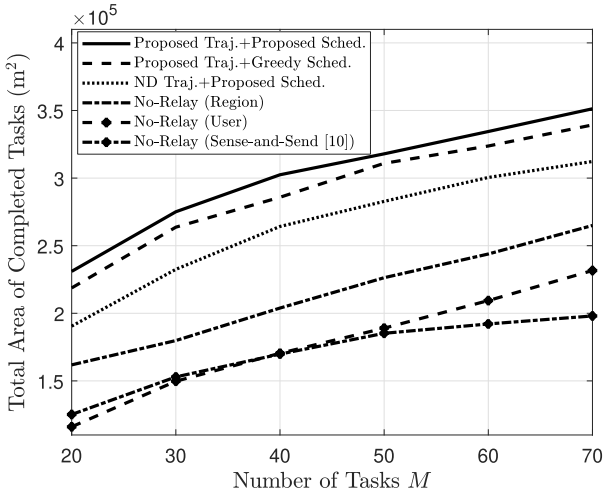

Fig. 11. Total area of completed tasks versus the number of tasks in the multiple-UAV case.

schemes, labeled "No-Relay (Region)" and "No-Relay (User)" in the figures, assign tasks to UAVs based on the locations of the surveillance regions and requesting users, respectively. That is, in the No-Relay (Region) scheme, UAV k serves only tasks in the set $\mathcal{M}_{\mathrm{I}}^{(k)}$ whereas, in the No-Relay (User) scheme, UAV k serves only tasks in the set $\mathcal{M}_{\mathrm{U}}^{(k)}$. The No-Relay (Sense-and-Send [10]) scheme considers a sequence of tasks that is the same as that of the No-Relay (Region) scheme, and the UAVs then serve their tasks following the Sense-and-Send [10] strategy adopted in the single-UAV case. The simulation results shown in this section are averaged over 60 network realizations.

In Fig. 10, we show the total area of completed tasks with respect to the UAVs' transmit SNR in the multiple-UAV case. We can see that the total area increases with the transmit SNR in all cases. While the proposed scheme performs the best at all SNRs, all relaying schemes are able to outperform non-relaying schemes due to the improved effectiveness of cross-UAV tasks through cooperation. By relaying images through other UAVs, each UAV need not fly far from its coverage area and, thus, can save time to serve more tasks. In contrast, UAVs in the non-relaying schemes may spend much time moving from surveillance regions to their requesting users, which can potentially be far away. Specifically, in the No-Relay (Region), UAVs only capture images of surveillance regions within their respective coverage areas but may need to travel outside their respective areas for delivery to the requesting users. The need to travel over long distances for data delivery may occur even more frequently in the No-Relay (Sense-and-Send [10]) due to its one-by-one task-serving strategy. In the No-Relay (User) scheme, UAVs may instead fly outside of their respective coverage areas to capture images but then must fly back to their respective areas for delivery. In all non-relaying schemes, UAVs may quickly run out of time serving tasks that require long travel distances and, thus, may be unable to complete many tasks before their deadlines. We can also observe that the advantage of relaying increases with the transmit SNR since inter-UAV transmissions can be completed more efficiently in this case, requiring less overhead for cooperation. Other than the proposed scheme, we can see that Greedy Sched. performs well at low SNR since obtaining a high transmission rate is critical for task completion in this case. ND Traj. performs well at high SNR since the UAV now has sufficient power to reach the requesting user or the relaying UAV, and, thus, choosing the nearest task reduces the travel time and allows more tasks to be completed.

In Fig. 11, we examine the performance with respect to the number of tasks M in the multiple-UAV case. In all cases, the total area of completed tasks increases with M. This is because, as the number of tasks increases, UAVs have more opportunity to complete tasks along their main path while simultaneously having more flexibility to perform task selection, similar to the single-UAV case. The proposed scheme is capable of optimally allocating time and communication resources to serve as many tasks as possible. The completion ratio (i.e., $\mu_m^{(k)}$) provides a useful guideline for adjusting the time needed by UAVs on the relay path to complete their local tasks. Moreover, by employing the completion ratio in the transmission causality constraint in (24f), cross-UAV tasks with low completion ratio will not be chosen by intermediate UAVs, which then can reallocate resources to other tasks. The non-relaying schemes are again worse than the relaying schemes since the challenge of completing tasks over long distances remains.

In Fig. 12, we show a realization of surveillance regions, requesting users, and the resulting UAV trajectories of the proposed scheme in the multiple-UAV case. In the multiple-UAV scenario, UAVs must design their trajectories, taking into account the need to capture images, receive images from neighboring UAVs, and send images to requesting users or neighboring UAVs. The intermediate UAVs may fly toward neighboring UAVs to enhance the UAV-to-UAV transmission rate while exchanging data for cross-UAV tasks. Once the last UAV on the relay path has received the data, it may also fly close to the requesting user to improve the data transmission rate. Notice that markers on the trajectories are provided to indicate when the UAV is transmitting directly to users of local tasks and when it is transmitting to a neighboring UAV. The

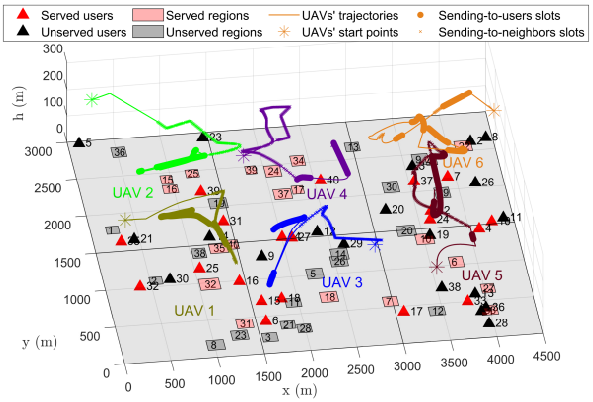

Fig. 12. Example of surveillance regions, requesting users, and the resulting UAV trajectories of the proposed scheme in the multiple-UAV case. Markers on the trajectories are provided to indicate when the UAV is transmitting directly to users of local tasks and when it is transmitting to a neighboring UAV.

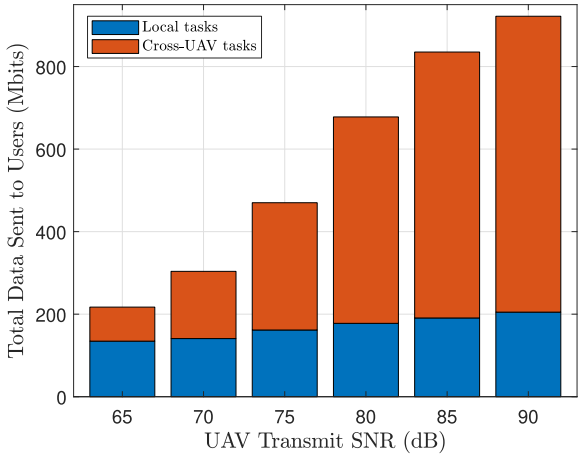

Fig. 13. Total image data (including that of local and cross-UAV tasks) that is delivered to the requesting users in the proposed scheme with respect to the transmit SNR.

illustration shows that the UAVs send data to users/neighboring UAVs at locations where they are close to the targets.

In Fig. 13, we show the average total image data that is eventually delivered to the requesting users with respect to the UAVs' transmit SNR. The total data is split into that of local tasks and that of cross-UAV tasks. The data corresponding to local tasks refers to data delivered by the UAV that captured the image, and that corresponding to cross-UAV tasks refers to data delivered through other UAVs. We can see that, at low SNR, UAVs tend to deliver less data through other UAVs since the inter-UAV transmission is less efficient in this case. However, as the transmit SNR increases, the inter-UAV transmission rates quickly improve, resulting in a rapid increase of the total data corresponding to cross-UAV tasks. The total data corresponding to local tasks increases much slower since the improvement in SNR is still insufficient to enable efficient transmission directly to a remote user without relaying.

VI. Conclusion

This work proposed a joint task assignment, transmission scheduling, and trajectory design for image surveillance UAVs to efficiently serve on-demand image capture and delivery services. We examined both single-UAV and multiple-UAV scenarios. The proposed designs were devised by maximizing the total area of completed tasks subject to constraints on image capture, image delivery, and deadlines. In the single-UAV case, we proposed an alternating optimization approach where the task assignment, transmission scheduling, and trajectory design were optimized in turn until convergence. We adopted EPM to promote near-binary solutions for the relaxed variables and SCA to deal with nonconvex trajectory optimization. Then, we extended our proposed scheme to the multiple-UAV scenario where cross-UAV tasks may require images to be captured and delivered by different UAVs. To enable distributed implementation, we utilized auxiliary deadlines to decouple the joint optimization problem into multiple single-UAV problems that can be solved in parallel. Numerical simulations showed significant improvements over baseline approaches based on ND/NL and greedy schemes and also demonstrated the benefit of relaying in the multiple-UAV scenario.

References

[1] X. Li and A. V. Savkin, "Networked unmanned aerial vehicles for surveillance and monitoring: A survey," *Future Internet*, vol. 13, no. 7, p. 174, Jul. 2021.

[2] X. Lei, X. Hu, G. Wang, and H. Luo, "A multi-UAV deployment method for border patrolling based on Stackelberg game," *J. Syst. Eng. Electron.*, vol. 34, no. 1, pp. 99–116, Feb. 2023.

[3] A. Raja, L. Njilla, and J. Yuan, "Adversarial attacks and defenses toward AI-assisted UAV infrastructure inspection," *IEEE Internet Things J.*, vol. 9, no. 23, pp. 23379–23389, Dec. 2022.

[4] P. K. R. Maddikunta et al., "Unmanned aerial vehicles in smart agriculture: Applications, requirements, and challenges," *IEEE Sensors J.*, vol. 21, no. 16, pp. 17608–17619, Aug. 2021.

[5] Y. Liang et al., "Nonredundant information collection in rescue applications via an energy-constrained UAV," *IEEE Internet Things J.*, vol. 6, no. 2, pp. 2945–2958, Apr. 2019.

[6] C. D. Franco and G. Buttazzo, "Coverage path planning for UAVs photogrammetry with energy and resolution constraints," *J. Intell. Robotic Syst.*, vol. 83, pp. 445–462, Feb. 2016.

[7] X.-W. Tang, S. Zhang, C. You, X.-L. Huang, and R. Zhang, "UAV-assisted image acquisition: 3D UAV trajectory design and camera control," in *Proc. IEEE 96th Veh. Technol. Conf. (VTC-Fall)*, Sep. 2022, pp. 1–6.

[8] N. Masmoudi, W. Jaafar, S. Cherif, J. B. Abderrazak, and H. Yanikomeroglu, "UAV-based crowd surveillance in post COVID-19 era," *IEEE Access*, vol. 9, pp. 162276–162290, 2021.

[9] N. Van Cuong, Y.-W. Peter Hong, and J.-P. Sheu, "UAV trajectory optimization for joint relay communication and image surveillance," *IEEE Trans. Wireless Commun.*, vol. 21, no. 12, pp. 10177–10192, Jun. 2022.

[10] S. Zhang, H. Zhang, B. Di, and L. Song, "Cellular cooperative unmanned aerial vehicle networks with sense-and-send protocol," *IEEE Internet Things J.*, vol. 6, no. 2, pp. 1754–1767, Apr. 2019.

[11] K. Meng et al., "Throughput maximization for UAV-enabled integrated periodic sensing and communication," *IEEE Trans. Wireless Commun.*, vol. 22, no. 1, pp. 671–687, Jan. 2023.

[12] M. Samir, S. Sharafeddine, C. M. Assi, T. M. Nguyen, and A. Ghrayeb, "UAV trajectory planning for data collection from time-constrained IoT devices," *IEEE Trans. Wireless Commun.*, vol. 19, no. 1, pp. 34–46, Jan. 2020.

[13] A. Mrad, A. Al-Hilo, S. Sharafeddine, and C. Assi, "NOMA-aided UAV data collection from time-constrained IoT devices," in *Proc. IEEE Int. Conf. Commun. (ICC)*, May 2022, pp. 1–6.

[14] C. Zhan, H. Hu, Z. Liu, Z. Wang, and S. Mao, "Multi-UAV-enabled mobile-edge computing for time-constrained IoT applications," *IEEE Internet Things J.*, vol. 8, no. 20, pp. 15553–15567, Apr. 2021.

[15] K. Liu and J. Zheng, "UAV trajectory optimization for time-constrained data collection in UAV-enabled environmental monitoring systems," *IEEE Internet Things J.*, vol. 9, no. 23, pp. 24300–24314, Dec. 2022.

[16] D. Tran, V. Nguyen, S. Chatzinotas, T. X. Vu, and B. Ottersten, "UAV relay-assisted emergency communications in IoT networks: Resource allocation and trajectory optimization," *IEEE Trans. Wireless Commun.*, vol. 21, no. 3, pp. 1621–1637, Mar. 2022.

[17] T. Kim and D. Qiao, "Energy-efficient data collection for IoT networks via cooperative multi-hop UAV networks," *IEEE Trans. Veh. Technol.*, vol. 69, no. 11, pp. 13796–13811, Sep. 2020.

[18] A. M. Almasoud, M. Y. Selim, A. Alqasir, T. Shabnam, A. Masadeh, and A. E. Kamal, "Energy efficient data forwarding in disconnected networks using cooperative UAVs," in *Proc. IEEE Global Commun. Conf. (GLOBECOM)*, Dec. 2018, pp. 1–6.

[19] J. Scherer and B. Rinner, "Multi-UAV surveillance with minimum information idleness and latency constraints," *IEEE Robot. Autom. Lett.*, vol. 5, no. 3, pp. 4812–4819, Jul. 2020.

[20] K. Meng, X. He, Q. Wu, and D. Li, "Multi-UAV collaborative sensing and communication: Joint task allocation and power optimization," *IEEE Trans. Wireless Commun.*, vol. 22, no. 6, pp. 4232–4246, Dec. 2023.

[21] N. Kumar, M. Ghosh, and C. Singhal, "UAV network for surveillance of inaccessible regions with zero blind spots," in *Proc. IEEE Conf. Comput. Commun. Workshops (INFOCOM WKSHPS)*, Jul. 2020, pp. 1213–1218.

[22] Meetha. V. Shenoy, A. Roy, and S. Misra, "QoI-aware camera network-as-a-service for social behavior analysis," in *Proc. IEEE Int. Conf. Commun. (ICC)*, Jun. 2021, pp. 1–6.

[23] A. Meng, X. Gao, Y. Zhao, and Z. Yang, "Three-dimensional trajectory optimization for energy-constrained UAV-enabled IoT system in probabilistic LoS channel," *IEEE Internet Things J.*, vol. 9, no. 2, pp. 1109–1121, Jan. 2022.

[24] C. You and R. Zhang, "Hybrid offline-online design for UAV-enabled data harvesting in probabilistic LoS channels," *IEEE Trans. Wireless Commun.*, vol. 19, no. 6, pp. 3753–3768, Jun. 2020.

[25] G. Yuan and B. Ghanem, "An exact penalty method for binary optimization based on MPEC formulation," in *Proc. 31st AAAI Conf. Artif. Intell. (AAAI)*, 2017, pp. 2867–2875.

[26] M. Grant and S. Boyd. (Jan. 2020). *CVX: MATLAB Software for Disciplined Convex Programming, Version 2.2*. [Online]. Available: http://cvxr.com/cvx/

[27] T. Ma et al., "UAV-LEO integrated backbone: A ubiquitous data collection approach for B5G Internet of Remote Things networks," *IEEE J. Sel. Areas Commun.*, vol. 39, no. 11, pp. 3491–3505, Nov. 2021.

[28] T. H. Cormen, C. E. Leiserson, R. L. Rivest, and C. Stein, *Introduction to Algorithms*, 2nd ed. Cambridge, MA, USA: MIT Press, 2001.

[29] Y.-W. P. Hong, R. Cheng, Y. Hsiao, and J. Sheu, "Power-efficient trajectory adjustment and temporal routing for multi-UAV networks," *IEEE Trans. Green Commun. Netw.*, vol. 4, no. 4, pp. 1106–1119, Dec. 2020.

[30] F. Diara and M. Roggero, "Quality assessment of DJI zenmuse L1 and P1 LiDAR and photogrammetric systems: Metric and statistics analysis with the integration of trimble SX10 data," *Geomatics*, vol. 2, no. 3, pp. 254–281, Jul. 2022.

[31] CENELEC, *Video Surveillance Systems for Use in Security Applications*, European Committee for Electrotechnical Standardization, Standard CENELEC EN 62676-4:2015, 2015.

Nguyen Van Cuong (Member, IEEE) received the B.S. degree in telecommunication-electronics engineering technology from Dalat University, Vietnam, in 2011, and the Ph.D. degree in communications engineering from National Tsing Hua University, Taiwan, in 2023. He is currently a Post-Doctoral Research Fellow with the Department of Computer Science, National Tsing Hua University. His research interests include wireless communications, the IoT and sensor networks, UAV communications, and machine learning for communications.

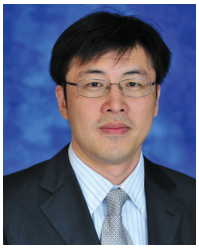

Y.-W. Peter Hong (Senior Member, IEEE) received the B.S. degree in electrical engineering from National Taiwan University, Taipei, Taiwan, in 1999, and the Ph.D. degree in electrical engineering from Cornell University, Ithaca, NY, USA, in 2005.

He joined the Institute of Communications Engineering and the Department of Electrical Engineering, National Tsing Hua University (NTHU), Hsinchu, Taiwan, in 2005, where he is currently a Full Professor and the Associate Dean of the College of EECS. His research interests include UAV communications, distributed signal processing for IoT and sensor networks, machine learning for wireless communications, and physical layer security. He received the IEEE ComSoc Asia-Pacific Outstanding Young Researcher Award in 2010, the Y. Z. Hsu Scientific Paper Award in 2011, the National Science Council Wu Ta-You Memorial Award in 2011, Chinese Institute of Electrical Engineering (CIEE) Outstanding Young Electrical Engineer Award in 2012, and the Ministry of Science and Technology Outstanding Research Award in 2018 and 2022. He was the Chair of the IEEE ComSoc Taipei Chapter from 2017 to 2018 and the Co-Chair of the Technical Affairs Committee, the Information Services Committee, and the Chapter Coordination Committee of the IEEE ComSoc Asia-Pacific Board from 2014 to 2015, from 2016 to 2019, and from 2020 to 2021, respectively. He serves as a Senior Area Editor for IEEE TRANSACTIONS ON SIGNAL PROCESSING. In the past, he also served as an Associate Editor for IEEE TRANSACTIONS ON SIGNAL PROCESSING and IEEE TRANSACTIONS ON INFORMATION FORENSICS AND SECURITY and an Editor for IEEE TRANSACTIONS ON COMMUNICATIONS. He was a Distinguished Lecturer of the IEEE Communications Society from 2022 to 2023. He is also the Vice Director of the IEEE ComSoc Asia-Pacific Board from 2022 to 2025.

Jang-Ping Sheu (Fellow, IEEE) received the B.S. degree in computer science from Tamkang University, Taiwan, in 1981, and the M.S. and Ph.D. degrees in computer science from National Tsing Hua University, Taiwan, in 1983 and 1987, respectively. He was the Director of the Department of Computer Science and Information Engineering, National Central University, from 1997 to 1999. He was the Director of the Computer Center, National Central University, from 2003 to 2006. He was the Director of the Computer and Communication Research Center, National Tsing Hua University, from 2009 to 2015. He was the Associate Dean of the College of Electrical and Computer Science, National Tsing Hua University, from 2016 to 2017. He is currently a Chair Professor with the Department of Computer Science and the Director of the Joint Research Center of Delta-NTHU, National Tsing Hua University. His current research interests include wireless communications, mobile computing, the Internet of Things, and UAV-assisted communication systems. He is an Advisory Board Member of *International Journal of Ad Hoc and Ubiquitous Computing* and *International Journal of Vehicle Information and Communication Systems*. He is a Phi Tau Phi Society Member. He received the Distinguished Research Awards of the National Science Council of Republic of China from 1993 to 1994, from 1995 to 1996, and from 1997 to 1998. He received the Distinguished Engineering Professor Award from Chinese Institute of Engineers in 2003. He received the K.-T. Li Research Breakthrough Award of the Institute of Information and Computing Machinery (IICM) in 2007. He received the Y. Z. Hsu Scientific Chair Professor Award and the Pan Wen Yuan Outstanding Research Award in 2009 and 2014, respectively. He received the Academic Award in Engineering from the Ministry of Education in 2016. He received the Medal of Honor in Information Sciences from IICM 2017. He received the TECO Award and Chinese Institute of Electrical Engineering (CIEE) Fellow in 2019 and 2021. He was an Associate Editor of IEEE TRANSACTIONS ON PARALLEL AND DISTRIBUTED SYSTEMS and *International Journal of Sensor Networks*.